Feature Alignment with Equivariant Convolutions for Burst Image Super-Resolution

Anonymous Author(s)
Affiliation
Address
email

Abstract

Burst image processing (BIP), which captures and integrates multiple frames into a single high-quality image, is widely used in consumer cameras. As a typical BIP task, Burst Image Super-Resolution (BISR) has achieved notable progress through deep learning in recent years. Existing BISR methods typically involve three key stages: alignment, upsampling, and fusion, often in varying orders and implementations. Among these stages, alignment is particularly critical for ensuring accurate feature matching and further reconstruction. However, existing methods often rely on techniques such as deformable convolutions and optical flow to realize alignment, which either focus only on local transformations or lack theoretical grounding, thereby limiting performance. To alleviate these issues, we propose a novel framework for BISR, featuring an equivariant convolution-based alignment, ensuring consistent transformations between the image and feature domains. This enables the alignment transformation to be learned via explicit supervision in the image domain and easily applied in the feature domain in a theoretically sound way, effectively improving alignment accuracy. Additionally, we design an effective reconstruction module with advanced architectures for upsampling and fusion to obtain the final BISR result. Extensive experiments on BISR benchmarks show our superior performance in both quantitative metrics and visual quality.

1 Introduction

Image super-resolution is an important task in image processing. Conventionally, it's mainly dealt with in the context of Single Image Super Resolution (SISR) [1, 2] and significant progress has been made in the last decades. By the advances in image acquisition technologies, a new kind of super-resolution technique, Burst Image Super-Resolution (BISR) [3, 4] has emerged as an increasingly valuable alternative. Unlike SISR, BISR reconstructs a high-resolution (HR) image by leveraging a sequence of low-resolution (LR) images captured in rapid succession, making it inherently more robust to noise and artifacts. Despite its advantages, BISR faces significant challenges, including accurate alignment for handling motion variations and effective multi-frame fusion.

The general pipeline for BISR typically involves three key stages: alignment, upsampling, and fusion, with their order and implementation varying across methods. Among them, alignment plays a crucial role in addressing spatial misalignments between successive frames, enabling accurate feature matching and high-quality reconstruction. Early methods [5, 6] mainly relied on Deformable Convolution Networks (DCNs) [7] for alignment, owing to their strong ability in modeling spatial transformations. Recently, optical flow [8] was adopted in the BurstM [9] method, showing better feature alignment performance than DCN, leveraging its explicit supervision in the image domain and a stronger ability to capture global transformations. However, since the transformation is estimated in the image domain, it may not be strictly applicable to the feature space without further constraints on

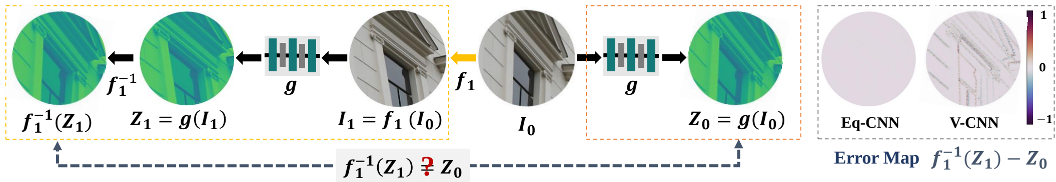

Figure 1: Illustration of transformation consistency in vanilla (V-CNN) and equivariant (Eq-CNN) convolutional networks. f_1 denotes a transformation (rotation in this example) and g is a CNN that extracts features from images. Suppose I_1 is the image obtained by applying f_1 to I_0, i.e., $I_1 = f_1(I_0)$, and Z_0 and Z_1 are features extracted from I_0 and I_1, respectively. We expect that Z_1 can be close to $f_1(Z_0)$, the affine transformation of Z_0, such that one can align Z_1 to Z_0 in the feature domain by applying the inverse transformation f_1^{-1}, which can be learned by explicit supervision in the image domain. The right box compares the error between $f_1^{-1}(Z_1)$ and Z_0, and it can be observed that Eq-CNN can more effectively achieve this goal than V-CNN.

the feature extractors, as intuitively illustrated in Figure 1. As a result, the feature alignment could be less accurate, as shown in Section 3.1, which negatively affects the final performance.

To alleviate the limitations of alignment in existing methods, we propose to leverage equivariant convolutional networks (Eq-CNNs) [10, 11, 12] with learnable transformation matrices as a solution. Compared with vanilla convolutional neural networks (V-CNNs) [13, 14], Eq-CNNs can extract features that are theoretically equivariant to input images under certain spatial transformations, e.g., rotation and translation. Then, if each source frame within burst images can be approximately modeled by an affine transformation (or more specifically, rotation plus translation) of the reference frame due to the acquisition mechanism [3], such a property of Eq-CNNS enables us to learn the transformation (or its inverse) with the image domain supervision and then apply the inverse transformation in the feature domain to achieve an easy while theoretically sound alignment from the source frame to the reference one, as illustrated in Figure 1.

With the aligned features as aforementioned, we further designed a reconstruction module for upsampling and fusion to generate the final sRGB image using advanced techniques. Specifically, considering its ability in capturing intricate inter-frame correlations, we adopt the Multi-Dconv Head Transposed Attention (MDTA) block [15] for feature interaction among frames; and due to its flexibility in multi-scale upsampling, we use the implicit neural representation (INR) technique [16] to upsample the features for final fusion, following [9].

To summarize, our contributions are as follows:

- We propose a new alignment framework for BISR based on Eq-CNN, which enables us to learn the alignment transformation with image domain supervision and apply it in the feature domain in a theoretically sound way. The corresponding theoretical analysis also advances the theory of Eq-CNN to a certain extent.
- We incorporate the proposed alignment framework with advanced techniques for upsampling and fusion, including Restomer and INR, and build a new deep model for BISR.
- We apply the proposed model to BISR benchmarks, demonstrate its superiority against current state-of-the-art methods.

2 Related Work

2.1 Burst image super-resolution

BISR and its related task, Muti Frame Super-Resolution (MFSR), have been extensively studied using both traditional approaches and deep learning techniques. The pioneering work by Tsai et al. [17] tackled the problem in the frequency domain, while subsequent research [18, 19, 20] put more focus on the spatial domain for resolution enhancement. With the rapid advances of deep learning, significant progress has been made. Initial studies [21, 22] employed relatively simple network architectures to address the MFSR task. Then, Bhat et al. [23] proposed a BISR pipeline

Table 1: Comparison of relative alignment error on $\times 4$ SyntheticBurst and BurstSR.

Dataset	Type	Domain	Flow	Ours
SyntheticBurst	synthetic	image	**0.18**	0.20
		feature	1.03	**0.94**
BurstSR	real	image	0.26	**0.17**
		feature	2.06	**1.94**

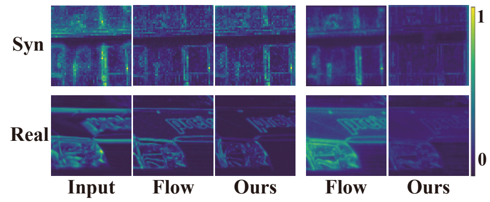

Figure 2: Error maps of aligned images (left) and features (right) .

incorporating alignment, feature fusion, and upsampling modules, together with the first real-world burst SR benchmark, inspiring numerous successive studies [24, 25, 5, 26, 6, 27, 28].

Within the BISR pipeline, alignment plays an important role, as highlighted by Kang et al. [9]. In previous methods [5, 6], DCN [7] is mainly adopted, but is insufficient for global transformation [9]. In contrast, Kang et al. [9] introduced optical flow [8] to achieve alignment, improving the performance. However, the image-domain estimated transformation may not be sufficient to achieve a theoretically sound and accurate feature alignment, motivating our development of a more principled alignment method via Eq-CNN.

In addition to alignment, fusion and upsampling have also benefited from recent architectural advances. Transformers [29] were used in [6, 26] for long-range modeling; QMambaBSR [28] introduced Mamba [30] for efficient sub-pixel integration; BSRD [27] employed diffusion models [31] for refined reconstruction; and BurstM [9] leveraged INRs [32, 16] for multi-scale upsampling.

2.2 Equivariant convolutions

One key factor behind the success of CNNs in computer vision is their inherent translation equivariance, which ensures spatial consistency. This principle has motivated the development of rotation-equivariant convolutions. GCNN [33] and HexaConv [34] enforce $\frac{\pi}{2}$ and $\frac{\pi}{3}$ rotational equivariance, while Xie et al. [35] extended this to near-continuous angles via Fourier-based filter parameterization, showing strong practical performance [12]. Leveraging such equivariance, Eq-CNN enables learning alignment transformations from image-domain supervision while preserving theoretical validity in the feature domain, which is an essential property in our alignment framework (see Section 3.1).

3 Proposed Method

We first discuss the motivation of our alignment framework for BISR. Then, we discuss the details of the proposed method. We also provide a theoretical justification for the validity of the proposed alignment framework.

3.1 Motivation

Alignment is a crucial component in the BISR pipeline. As discussed in the Introduction and Related Work, early deep learning approaches [5, 6] commonly employed DCN [7] for alignment. However, Kang et al. [9] pointed out that DCN struggles to capture global transformations and demonstrated that optical flow provides more effective feature alignment with supervision and global matching. Despite these advantages, the optical flow-based alignment has a theoretical limitation that should be noted. Specifically, the estimated transformations by optical flow are supervised in the image domain while applied in the feature domain, but there is no rigorous guarantee that the transformations of the two domains are consistent without further constraints on the feature extractor, as shown in Figure 1. To further investigate this issue, we compute the relative alignment error of BurstM, which uses the optical flow to align features, and compared with that of our method, as shown in Table 1 and Figure 2. It can be seen that both methods achieve comparable image alignment, but the feature alignment of optical flow is much worse.

To alleviate this issue, we propose a theoretically sound alignment approach based on Eq-CNN. We first briefly introduce the concept of equivariance in deep learning. Suppose g is a deep feature extractor mapping from input to the feature space and F is a transformation group, we say g is equivariant with respect to F if for any $f \in F$, it holds that $f(g(I)) = g(f(I))$, or equivalently,

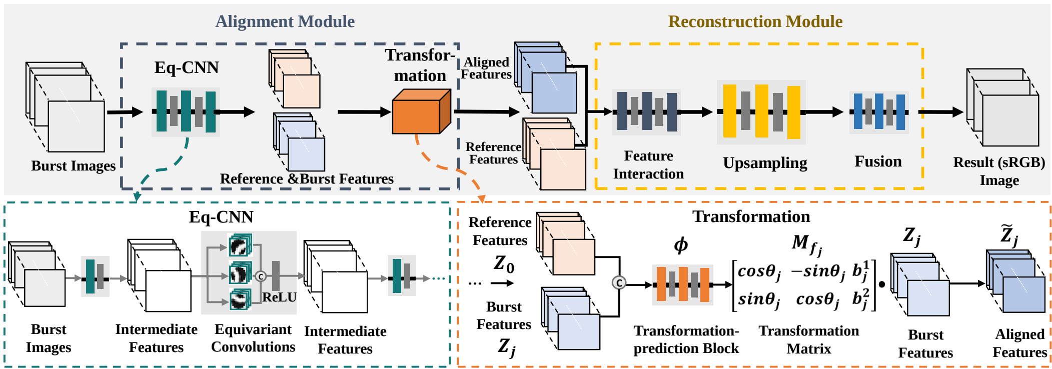

Figure 3: Overview of our proposed method. The top row shows the whole workflow. The bottom left shows the detailed equivariant convolution layers of Eq-CNN. The bottom right shows the process of feature alignment by predicted transformation, detailed in Section 3.2.2.

$g(I) = f^{-1}\big(g(f(I))\big)$ if f is invertible. Note that, we abuse the notation f a little to denote the same transformation applied in different domains. It is well known that V-CNNs are only equivariant under translation, while previous studies on equivariance [10, 35] constructed CNNs that are also equivariant with respect to rotation and reflection, which are often specifically referred to as Eq-CNNs.

This theoretical foundation of Eq-CNN allows us to design an alignment framework where a transformation (e.g., rotation and translation) estimated and supervised in the image domain remains valid in the feature domain. Considering that misalignments in burst images typically arise from slight camera shifts and can often be approximated by simple geometric transformations [3], such a rotation-translation modeling is reasonable. We leverage Eq-CNNs to extract features from input frames, and then apply explicit transformation matrices for alignment directly in the feature domain. The results in Table 1 and Figure 2 support this idea, that our method achieves a better feature alignment, especially on the real dataset.

3.2 Our method

3.2.1 Problem setting and processing pipeline

Given B low-resolution (LR) RAW burst frames $\{I_j^L\}_{j=0}^{B-1}$ with each $I_j^L \in \mathbb{R}^{h\times w\times 1}$, we first process it a 4-channel format following the RGGB Bayer pattern [9, 6]. Then, one frame is selected as the reference frame, which serves as the reference for high-resolution (HR) reconstruction, and the rest frames are used to assist the reference one in super-resolving. The reconstructed HR image $I^S \in \mathbb{R}^{sh\times sw\times 3}$ is in sRGB format, where s is the scale factor. As shown in Figure 3, our processing pipeline includes two main steps, i.e., alignment and reconstruction. The alignment step aims to extract and align features from the LR burst images using the Eq-CNN, and the reconstruction step tries to upsample and fuse the features to get the final reconstruction.

3.2.2 Alignment Module

Let I_0^L denote the RAW LR reference frame and $\{I_j^L\}_{j=1}^{B-1}$ represent the remaining source frames in the burst image. Following the discussions in Section 3.1, we approximately model the relationship between each I_j^L $(j \neq 0)$ and I_0^L as

$$I_j^L = f_j(I_0^L), \tag{1}$$

where f_j is a rotation-translation transformation. After feature extraction using an Eq-CNN g, we can obtain features $Z_0 = g(I_0)$ and $Z_j = g(I_j)$, respectively. Assuming the equivariance property of g strictly holds, we have that

$$Z_j = g(I_j) = g(f_j(I_0^L)) = f_j(g(I_0^L)) = f_j(Z_0). \tag{2}$$

This indicates if we can accurately estimate f_j or f_j^{-1} in the image domain, we can apply it to Z_j:

$$\tilde{Z}_j = f_j^{-1}(Z_j), \tag{3}$$

such that $\tilde{Z}_j$ is well algined to Z_0. Therefore, we learn f_j^{-1} via the image domain supervision with the following loss:

$$\mathcal{L}_{\text{align}} = \frac{1}{B-1} \sum_{j=1}^{B-1} \|f_j^{-1}(I_j^L) - I_0^L\|_2^2. \tag{4}$$

In practice, however, due to the discretization of the rotation angles in Eq-CNNs, we cannot strictly guarantee that $f_j^{-1}(Z_j) = Z_0$. Nevertheless, we can prove the following result:

Proposition 1. *For an images I_0 and I_j of size $H \times W \times n_0$, a rotation-translation Eq-CNN $g(\cdot)$ with discretized angles, and a rotation-translation transformation $f_j(\cdot)$, let $Z_0 = g(I_0)$ and $Z_j = g(I_j)$ be the feature maps, where $Z_0, Z_j \in \mathbb{R}^{H \times W \times tC}$, and then the following result holds:*

$$\|f_j^{-1}(Z_j) - Z_0\|_\infty \leq C_3 \left\|f_j^{-1}(I_j) - I_0\right\|_2 + C_1 h^2 + C_2 pht^{-1}, \tag{5}$$

where t, p, h, C_1, C_2, C_3 constants.

Proposition 1 suggests that we can minimize the distance between $f_j^{-1}(Z_j)$ and Z_0, the main goal of the Alignment module, through minimizing the distance between $f_j^{-1}(I_j^L)$ and I_0^L, which is we are trying to do by the loss defined in Eq. (4). The detailed version of Proposition 1 and its proof is are provided in Appendix A.4.

The next question is then how to parameterize the transformation f_j^{-1}. Since we assume f_j is a rotation-translation transformation following [3] as discussed in Section 3.1, its inverse f_j^{-1} is also a rotation-translation transformation, which can be parameterized using a matrix $M_{f_j} \in \mathbb{R}^{2\times 3}$:

$$M_{f_j} = \begin{bmatrix} \cos\theta_j & -\sin\theta_j & b_j^1 \\ \sin\theta_j & \cos\theta_j & b_j^2 \end{bmatrix}, \tag{6}$$

where θ_j is the rotation angle, and $\boldsymbol{b}_j = (b_j^1, b_j^2)^T$ is the translation vector. Then, a pixel at location $(x_1, x_2)^T$ will be mapped to a new location $(x_1', x_2')^T$ after applying f_j^{-1}:

$$\begin{bmatrix} x_1' \\ x_2' \end{bmatrix} = M_{f_j} \cdot \begin{bmatrix} x_1 \\ x_2 \\ 1 \end{bmatrix} = \begin{bmatrix} x_1 \cos\theta_j - x_2 \sin\theta_j + b_j^1 \\ x_1 \sin\theta_j + x_2 \cos\theta_j + b_j^2 \end{bmatrix}. \tag{7}$$

Then we further parameterize $\{\theta_j, \boldsymbol{b}_j\}$ using a network block ϕ, referred to as transformation prediction block in Figure 3, with Z_0, Z_j as its input:

$$\{\theta_j, \boldsymbol{b}_j\} = \phi\left(\text{concat}[Z_0, Z_j]\right), \tag{8}$$

such that we can directly predict the alignment transformation f_j^{-1} during inference.

3.2.3 Reconstruction Module

After alignment, the aligned features $\{\tilde{Z}_j\}_{j=0}^{B-1}$ of all frames (we let $\tilde{Z}_0 := Z_0$ for convenience) are then further processed for reconstructing the HR sRGB image.

Feature interaction. Before upsampling, feature interaction between reference and source frames is necessary for enriching frame information. Instead of concatenation [5, 6, 9] or pixel-wise attention [36], we adopt the MDTA block from Restormer [15], which performs channel-wise self-attention via cross-covariance, capturing global context and enabling more effective integration of reference-source features. The interaction process for the aligned features of all frames is as follows ($j = 0, \ldots, B-1$):

$$\mathbf{Q}_j = W_d^Q W_p^Q(\text{concat}[\tilde{Z}_j, \tilde{Z}_0]), \quad \mathbf{K}_j = W_d^K W_p^K(\text{concat}[\tilde{Z}_j, \tilde{Z}_0]), \tag{9}$$

$$\mathbf{V}_j = W_d^V W_p^V(\text{concat}[\tilde{Z}_j, \tilde{Z}_0]), \quad \hat{Z}_j = \mathbf{V}_j \cdot \text{Softmax}(\mathbf{K}_j \cdot \mathbf{Q}_j / \alpha_j) + \tilde{Z}_j, \tag{10}$$

where $\{\hat{Z}_j\}_{j=0}^{B-1}$ are the features after interaction, $W_p^{(\cdot)}$ and $W_d^{(\cdot)}$ refer to 1×1 pixel-wise and 3×3 depth-wise convolutions, respectively, and α_j is a learnable scaling parameter. The term $\text{Softmax}(\mathbf{K}_j \cdot \mathbf{Q}_j / \alpha_j)$ captures feature correlations and dynamically weights value vectors based on similarity, enabling context-aware fusion.

Upsampling and fusion. For upsampling, we adopt the LTE framework [16], utilizing INR and frequency domain processing to recover high-frequency details. LTE offers two key advantages for

BISR: (1) It enables multi-scale upsampling [9], allowing a single model to cover diverse scenarios; (2) Its grid sampling mechanism effectively recovers sub-pixel information, crucial for burst images with subtle camera shifts. After upsampling, we use a fusion block with channel attention to integrate the upscaled features, along with a skip connection to preserve reference frame information. To be specific, the upsampling and final fusion process can be formulated as

$$I^S = \text{PS}\left(\tilde{I}_0^L \uparrow + \text{Avg}_W\left(\{\Phi_{\text{up}_j}(\hat{Z}_j)\}_{j=0}^{B-1}\right)\right), \ \ \tilde{I}_0^L \uparrow = \text{Conv}_{1\times1}(\text{Up}[I_0^L], . \tag{11}$$

where $I^S \in \mathbb{R}^{sh\times sw\times 3}$ is the final output in sRGB format, $\text{PS}(\cdot)$ denotes the pixel shuffle operation, $\text{Avg}_W(\cdot)$ refers to the weighted average operation with parameters learned via convolutions from $\hat{Z}_j$s, $\Phi_{\text{up}_j}(\cdot)$ denotes the LTE-based upsampling, $\tilde{I}_0^L \uparrow \in \mathbb{R}^{(sh/2)\times(sw/2)\times 12}$, $\text{Up}[\cdot]$ refers to the bilinear upsampling operation, and $\text{Conv}_{1\times1}(\cdot)$ is a 1×1 convolution layer.

3.2.4 Training loss

The whole network is trained in an end-to-end way using the following loss:

$$\mathcal{L} = \mathcal{L}_{\text{align}} + \mathcal{L}_{\text{fidelity}} = \mathcal{L}_{\text{align}} + \left\|I^S - I^{\text{GT}}\right\|_1, \tag{12}$$

where $\mathcal{L}_{\text{align}}$ is defined in Eq. (4), and I^{GT} the ground truth HR sRGB image.

3.3 Theoretical results

This section provides further discussions on the theoretical aspects of our method, and the readers who are not interested in the theory of Eq-CNN can just skip it. As mentioned in Section 3.2.2, Proposition 1 theoretically guarantee the reasonability of our feature alignment strategy. However, its proof is not trivial and relies on the following theorem:

Theorem 1. *For an image I_0 of size $H\times W\times n_0$, a rotation-translation Eq-CNN $g(\cdot)$ with discretized angles, and a rotation-translation transformation $f_j(\cdot)$, under certain conditions, the following result holds:*

$$\|f_j^{-1}\big(g(f_j(I_0))\big) - g(I_0)\|_\infty \le C_1 h^2 + C_2 pht^{-1}, \tag{13}$$

where t, p, h, C_1, C_2 are constants.

Different from existing theories in Eq-CNN showing that input transformations can be predictably reflected in the feature domain, by measuring the error between $g(f_j(I_0))$ and $f_j(g(I_0))$, Theorem 1 further analyzes the residual errors caused by inverse transformation applied to these two objects in discrete settings of Eq-CNN, and suggests that such an error can also be upper-bounded. Such an analysis provides a theoretical understanding of how input-level inverse transformations affect feature relationships, which advances the theory of Eq-CNN to a certain extent. The detailed version of Theorem 1 and its proof are in Appendix A.3.

4 Experiments

In this section, we conduct experiments to validate the effectiveness of our proposed method. We first evaluate the proposed method on standard benchmarks for BSIR in comparison with existing methods. Then, we conduct ablation studies to demonstrate the reasonablity of our method, specifically concerning the alignment mechanism.

4.1 Experiments on BISR benchmarks

4.1.1 Settings

Datasets. We follow previous studies [6, 9] and conduct experiments on two datasets: **(1) SyntheticBurst Dataset** [3], which consists of 46,839 burst sequences for training and 300 for validation. Each burst sequence contains 14 RAW LR frames generated from an HR sRGB image using the standard pipeline [5, 9]. Specifically, unprocessing techniques [37] are firstly applied to simulate RAW sensor data, and random rotations and translations are implemented to simulate real camera motion. Following [9], we generate multi-scale LR images through random down-sampling (×2, ×3, ×4). Finally, Bayer mosaicking and random noise are added to more closely reproduce real-world imaging conditions. **(2) BurstSR Dataset** [23], which comprises 200 full-size RAW burst sequences, with 5,405 patches of size 80×80 extracted for training and 882 patches for validation. The LR images

Table 2: Quantitative results on SyntheticBurst and BurstSR datasets. The best and second-best results are highlighted in bold and underlined, respectively.

Method	SyntheticBurst						BurstSR		BurstSR	
	x2		x3		x4		x4		Params.(M)	FLOPs(G)
	PSNR	SSIM	PSNR	SSIM	PSNR	SSIM	PSNR	SSIM		
Bicubic	38.30	0.948	33.94	0.886	33.02	0.862	42.55	0.962	-	-
DBSR [23]	40.51	0.965	40.11	0.959	40.76	0.959	48.05	0.984	13.01	111.71
MFIR [24]	41.25	0.971	41.81	0.972	41.56	0.964	48.33	0.985	12.13	121.01
BIPNet [5]	37.58	0.928	40.83	0.955	41.93	0.960	48.49	0.985	6.7	326.47
Burstormer [6]	37.06	0.925	40.26	0.953	42.83	0.973	48.06	0.986	2.5	38.33
GMTNet [26]	-	-	-	-	42.36	0.961	48.95	0.986	-	300
BSRT-Small [25]	40.64	0.966	42.30	0.975	42.72	0.971	48.57	0.986	4.92	178.82
BSRT-Large [25]	40.33	0.965	42.87	0.979	**43.62**	**0.975**	48.57	0.986	20.71	362.63
BurstM [9]	46.01	**0.985**	44.79	0.982	42.87	0.973	49.12	**0.987**	14.0	436.21
Ours	**46.10**	**0.985**	**44.95**	**0.983**	43.18	0.974	**49.22**	**0.987**	8.7	170.21

BIPNet Burstormer BSRT-L BurstM Ours GT

Figure 4: Visual comparison of x4 BISR on the SyntheticBurst dataset.

are captured using a smartphone, while the HR ground truth images are obtained from a DSLR under the same scenes. Each LR burst sequence consists of 14 frames, and the scale factor between LR and HR images in this dataset is fixed (×4).

Competing methods and evaluation metrics. We evaluate our method against 8 representative ones, including traditional Bicubic interpolation and current state-of-the-art methods for the BISR task: DBSR [23], MFIR [24], BIPNet [5], GMTNet [26], Burstormer [6], BSRT [25], and BurstM [9]. We employ two widely used metrics, PSNR and SSIM, to quantitatively assess the reconstruction quality of each method. Additionally, we report model complexity metrics, including the number of parameters and GFLOPs, to show the computational efficiency of each method as a reference.

Implementation details. All experiments are implemented using PyTorch on an NVIDIA 4090 GPU. For the SyntheticBurst dataset, the initial learning rate is set to 1×10^{-4} and gradually adjusted to 1×10^{-6} over 300 epochs. The batch size is set to 1, and the patch size is 48×48. For the BurstSR dataset, we fine-tune the model pre-trained on SyntheticBurst following [9], using an initial learning rate of 1×10^{-5} and CosineAnnealingLR to adjust it to 1×10^{-6} over 30 epochs. The batch size is 1, and the patch size is 80×80. For other compared deep learning-based methods, we test using the author-released models, except GMTNet for which we directly quote the results reported in the original paper since the model is not released.

4.1.2 Results

Results on SyntheticBurst Dataset [3]. We present the quantitative and qualitative evaluation results in Table 2 and Fig. 4, respectively, with full-size and additional visual results available in Appendix B because of space limitations.

As shown in Table 2, our method outperforms existing BISR approaches across nearly all evaluation metrics. Specifically, for the widely-used ×4 SR setting, our method achieves the results with a PSNR of 43.18 and an SSIM of 0.974, surpassing competing methods with comparable model complexities. This quantitatively demonstrates its effectiveness in reconstructing the original HR sRGB image.

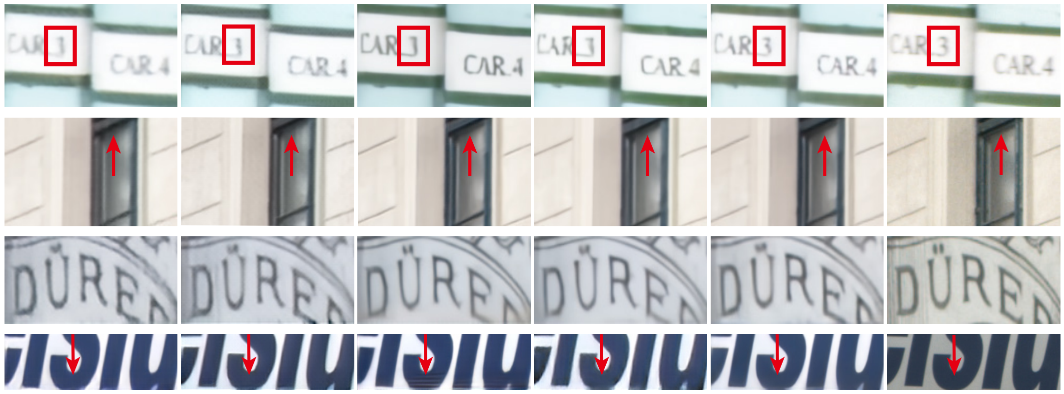

Figure 5: Visual comparison of x4 BISR on the BurstSR dataset.

Notably, our approach outperforms the current state-of-the-art multi-scale BISR method BurstM [9] while requiring fewer parameters and less FLOPs, showing both its efficiency and effectiveness. Furthermore, our method consistently performs well across different SR factor settings, suggesting its promising generalization ability. Visual results in Fig. 4 show that our method achieves competitive performance in several aspects. For example, our approach better preserves fine-grained textual details while maintaining structural fidelity. In addition, the method shows its ability to suppress noise without introducing unexpected artifacts or severe color distortions. These qualitative advantages of our method are consistent with its quantitative performance. It should be mentioned that though our model achieves slightly lower numeric results due to its fewer parameters (8.7M) compared to BSRT-Large (20.71M), it delivers comparable visual quality. Additional visual results of other scales are provided in the supplementary material for a more comprehensive comparison.

Results on BurstSR Dataset. The quantitative results on the BurstSR dataset are summarized in Table 2. It can be seen that our method achieves the best performance in terms of both PSNR and SSIM among all competing ones. Note that, in this real dataset, although the degradation process of the LR burst images is unknown, and the relationship between the source and reference frames might not be more complex than assumed, our method still performs promisingly. This indicates that, though relatively simple, the rotation-translation assumption for the align transformation made in our model is rational and effective in real scenarios.

The visual results in Fig. 5 further validate the effectiveness of our approach. Overall, our method keeps more fine-grained details and produces fewer unexpected artifacts compared with existing methods. For example, as shown in the first row, our result better keeps the morphology of characters and digital numbers, and in the last row, our method can better suppress artifacts while producing relatively sharper edges. More visual results on this dataset are provided in the Appendices.

4.2 Ablation Study

In this subsection, we conduct experiments on the SyntheticBurst dataset at ×4 scale to validate the rationality and effectiveness of the proposed alignment framework in our model. The overall quantitative and visual results are summarized in Table 3 and shown in Fig. 6 - Fig. 7, respectively.

Effectiveness of the overall alignment module (a) & (b). We first replace the whole alignment module in our method with implicit alignment strategies using Restormer (a) and deformable convolutions (b). As shown in Table 3, both methods exhibit significant performance degradation, which can be more intuitively observed in the visual results illustrated in Fig. 6 (a) and (b), that the fine-grained textures are not well kept. This can be attributed to the misalignment of features, as can be observed in Fig. 7 (a) and (b). These results clearly substantiate the effectiveness of our alignment module.

Effectiveness of equivariant feature extraction (c). We then conduct an ablation study by replacing the ENet, which is an Eq-CNN, with a V-CNN without the rotation equivariance for feature extraction. As shown in Table 3 (c) and Fig. 6 (c), this variant exhibits a noticeable performance drop compared to the proposed model in quantitative metrics and also produces blurry textures. The reason can be attributed to the lack of consistency of the alignment transformations between the image and feature domains, leading to mismatching among aligned features. Another interesting observation

Figure 6: Visualization of the ablation for $\times 4$ BISR on SyntheticBurst. Settings (a)-(d) are in Table 3.

Table 3: Ablation Study on $\times 4$ SyntheticBurst

Settings	PSNR	SSIM	Params.(M)
(a) Align with RT	42.97	0.972	9.0
(b) Align with DConv	42.81	0.970	11.5
(c) w/o Eq-CNN	42.76	0.971	10.1
(d) w/o T-mat.	42.80	0.972	8.7
Ours	43.18	0.974	8.7

**RT: Restormer [15]*
**DConv: Deformable convolution network [7]*
**w/o Eq-CNN: Replacing Eq-CNN with V-CNN*
**w/o T-mat: Removing the transformation matrix*

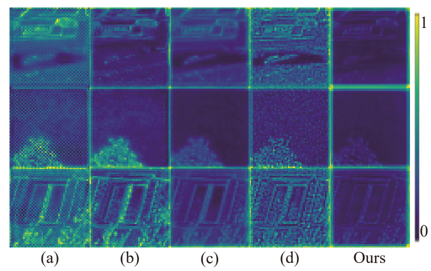

Figure 7: Error maps of aligned features for ablation studies on ×4 burst super-resolution using the SyntheticBurst dataset. Detailed settings of (a)-(d) can be referred to Table 3 and Section 4.2.

is that, though it does not perform well in the quantitative metrics, the visual results of this variant are comparable or even look better than that of other ablation variants as shown in Fig. 6, and the alignment error in features is also significantly smaller than that of variants (a) and (b) as depicted in Fig. 7. This can be due to the explicit alignment mechanism using the learnable transformation and the translation-equivariance of V-CNNs, which indirectly suggests the effectiveness of our approach.

Effectiveness of the learnable transformation matrix (d). We then remove the transformation matrix, denoted as "w/o T-mat." in Table 3, and such a variant can be seen as implementing implicit alignment with the Eq-CNN. It can be observed from Fig. 7 (d) that this leads to obvious feature misalignment and correspondingly inferior performance both in quantitative metrics and visual effects, highlighting the crucial role of explicit alignment.

5 Conclusion and Limitation

In this work, we have proposed a new method for BISR. The key consideration of our method is that we have designed a new effective alignment framework for the BISR task with Eq-CNN. Within the proposed alignment framework, by the equivariance property of Eq-CNN, the align transformation can be learned with explicit image domain supervision and directly applied in the feature domain in a theoretically sound way. In addition, we have introduced effective upsampling and fusion blocks using advanced neural architectures, including MDTA from Restormer and INR. Extensive experiments on two representative BISR benchmarks have been conducted, showing the effectiveness of the proposed method, both quantitatively and visually, against current state-of-the-art methods.

Despite its promising performance for BISR, our method still has limitations that need further investigation. For example, currently, the transformation considered in our model is restricted to rotation and translation due to the ability of existing Eq-CNNs, which may not be precise enough to characterize the relationship between the reference and source frame in complex real-world scenarios. Tackling this issue requires developing new techniques and theories for equivariance networks, which could not only enhance the availability of our method in real applications but also advance the study of equivariance in deep learning.

References

[1] Zhihao Wang, Jian Chen, and Steven CH Hoi. Deep learning for image super-resolution: A survey. *IEEE transactions on pattern analysis and machine intelligence*, 43(10):3365–3387, 2020.

[2] Chao Dong, Chen Change Loy, Kaiming He, and Xiaoou Tang. Image super-resolution using deep convolutional networks. *IEEE transactions on pattern analysis and machine intelligence*, 38(2):295–307, 2015.

[3] Goutam Bhat, Martin Danelljan, and Radu Timofte. Ntire 2021 challenge on burst super-resolution: Methods and results. In *Proceedings of the IEEE/CVF Conference on Computer Vision and Pattern Recognition*, pages 613–626, 2021.

[4] Goutam Bhat, Martin Danelljan, Radu Timofte, Yizhen Cao, Yuntian Cao, Meiya Chen, Xihao Chen, Shen Cheng, Akshay Dudhane, Haoqiang Fan, et al. Ntire 2022 burst super-resolution challenge. In *Proceedings of the IEEE/CVF conference on computer vision and pattern recognition*, pages 1041–1061, 2022.

[5] Akshay Dudhane, Syed Waqas Zamir, Salman Khan, Fahad Shahbaz Khan, and Ming-Hsuan Yang. Burst image restoration and enhancement. In *Proceedings of the ieee/cvf Conference on Computer Vision and Pattern Recognition*, pages 5759–5768, 2022.

[6] Akshay Dudhane, Syed Waqas Zamir, Salman Khan, Fahad Shahbaz Khan, and Ming-Hsuan Yang. Burstormer: Burst image restoration and enhancement transformer. In *2023 IEEE/CVF Conference on Computer Vision and Pattern Recognition (CVPR)*, pages 5703–5712. IEEE, 2023.

[7] Jifeng Dai, Haozhi Qi, Yuwen Xiong, Yi Li, Guodong Zhang, Han Hu, and Yichen Wei. Deformable convolutional networks. In *Proceedings of the IEEE international conference on computer vision*, pages 764–773, 2017.

[8] Berthold KP Horn and Brian G Schunck. Determining optical flow. *Artificial intelligence*, 17(1-3):185–203, 1981.

[9] EungGu Kang, Byeonghun Lee, Sunghoon Im, and Kyong Hwan Jin. Burstm: Deep burst multi-scale sr using fourier space with optical flow. In *European Conference on Computer Vision*, pages 459–477. Springer, 2025.

[10] Maurice Weiler, Fred A Hamprecht, and Martin Storath. Learning steerable filters for rotation equivariant cnns. In *Proceedings of the IEEE Conference on Computer Vision and Pattern Recognition*, pages 849–858, 2018.

[11] Qi Xie, Qian Zhao, Zongben Xu, and Deyu Meng. Fourier series expansion based filter parametrization for equivariant convolutions. *IEEE Transactions on Pattern Analysis and Machine Intelligence*, 45(4):4537–4551, 2022.

[12] Jiahong Fu, Qi Xie, Deyu Meng, and Zongben Xu. Rotation equivariant proximal operator for deep unfolding methods in image restoration. *IEEE Transactions on Pattern Analysis and Machine Intelligence*, 2024.

[13] Alex Krizhevsky, Ilya Sutskever, and Geoffrey E Hinton. Imagenet classification with deep convolutional neural networks. *Advances in neural information processing systems*, 25, 2012.

[14] Bee Lim, Sanghyun Son, Heewon Kim, Seungjun Nah, and Kyoung Mu Lee. Enhanced deep residual networks for single image super-resolution. In *Proceedings of the IEEE conference on computer vision and pattern recognition workshops*, pages 136–144, 2017.

[15] Syed Waqas Zamir, Aditya Arora, Salman Khan, Munawar Hayat, Fahad Shahbaz Khan, and Ming-Hsuan Yang. Restormer: Efficient transformer for high-resolution image restoration. In *Proceedings of the IEEE/CVF conference on computer vision and pattern recognition*, pages 5728–5739, 2022.

[16] Jaewon Lee and Kyong Hwan Jin. Local texture estimator for implicit representation function. In *Proceedings of the IEEE/CVF conference on computer vision and pattern recognition*, pages 1929–1938, 2022.

[17] Roger Y Tsai and Thomas S Huang. Multiframe image restoration and registration. *Multiframe image restoration and registration*, 1:317–339, 1984.

[18] Michal Irani and Shmuel Peleg. Improving resolution by image registration. *CVGIP: Graphical models and image processing*, 53(3):231–239, 1991.

[19] Hanoch Ur and Daniel Gross. Improved resolution from subpixel shifted pictures. *CVGIP: Graphical models and image processing*, 54(2):181–186, 1992.

[20] M. Elad and A. Feuer. Restoration of a single superresolution image from several blurred, noisy, and undersampled measured images. *IEEE Transactions on Image Processing*, 6(12):1646–1658, 1997.

[21] Evgeniya Ustinova and Victor Lempitsky. Deep multi-frame face super-resolution. *arXiv preprint arXiv:1709.03196*, 2017.

[22] Andrea Bordone Molini, Diego Valsesia, Giulia Fracastoro, and Enrico Magli. Deepsum: Deep neural network for super-resolution of unregistered multitemporal images. *IEEE Transactions on Geoscience and Remote Sensing*, 58(5):3644–3656, 2019.

[23] Goutam Bhat, Martin Danelljan, Luc Van Gool, and Radu Timofte. Deep burst super-resolution. In *Proceedings of the IEEE/CVF conference on computer vision and pattern recognition*, pages 9209–9218, 2021.

[24] Goutam Bhat, Martin Danelljan, Fisher Yu, Luc Van Gool, and Radu Timofte. Deep reparametrization of multi-frame super-resolution and denoising. In *Proceedings of the IEEE/CVF international conference on computer vision*, pages 2460–2470, 2021.

[25] Ziwei Luo, Youwei Li, Shen Cheng, Lei Yu, Qi Wu, Zhihong Wen, Haoqiang Fan, Jian Sun, and Shuaicheng Liu. Bsrt: Improving burst super-resolution with swin transformer and flow-guided deformable alignment. In *Proceedings of the IEEE/CVF Conference on Computer Vision and Pattern Recognition*, pages 998–1008, 2022.

[26] Nancy Mehta, Akshay Dudhane, Subrahmanyam Murala, Syed Waqas Zamir, Salman Khan, and Fahad Shahbaz Khan. Gated multi-resolution transfer network for burst restoration and enhancement. In *2023 IEEE/CVF Conference on Computer Vision and Pattern Recognition (CVPR)*, pages 22201–22210. IEEE, 2023.

[27] Kyotaro Tokoro, Kazutoshi Akita, and Norimichi Ukita. Burst super-resolution with diffusion models for improving perceptual quality. *arXiv preprint arXiv:2403.19428*, 2024.

[28] Xin Di, Long Peng, Peizhe Xia, Wenbo Li, Renjing Pei, Yang Cao, Yang Wang, and Zheng-Jun Zha. Qmambabsr: Burst image super-resolution with query state space model. *arXiv preprint arXiv:2408.08665*, 2024.

[29] A Vaswani. Attention is all you need. *Advances in Neural Information Processing Systems*, 2017.

[30] Albert Gu and Tri Dao. Mamba: Linear-time sequence modeling with selective state spaces. *arXiv preprint arXiv:2312.00752*, 2023.

[31] Jonathan Ho, Ajay Jain, and Pieter Abbeel. Denoising diffusion probabilistic models. *Advances in neural information processing systems*, 33:6840–6851, 2020.

[32] Yinbo Chen, Sifei Liu, and Xiaolong Wang. Learning continuous image representation with local implicit image function. In *Proceedings of the IEEE/CVF conference on computer vision and pattern recognition*, pages 8628–8638, 2021.

[33] Taco Cohen and Max Welling. Group equivariant convolutional networks. In *International conference on machine learning*, pages 2990–2999. PMLR, 2016.

[34] Emiel Hoogeboom, Jorn WT Peters, Taco S Cohen, and Max Welling. Hexaconv. *arXiv preprint arXiv:1803.02108*, 2018.

[35] Qi Xie, Qian Zhao, Zongben Xu, and Deyu Meng. Fourier series expansion based filter parametrization for equivariant convolutions. *IEEE Transactions on Pattern Analysis and Machine Intelligence*, 45(4):4537–4551, 2022.

[36] Pengxu Wei, Yujing Sun, Xingbei Guo, Chang Liu, Guanbin Li, Jie Chen, Xiangyang Ji, and Liang Lin. Towards real-world burst image super-resolution: Benchmark and method. In *Proceedings of the IEEE/CVF International Conference on Computer Vision*, pages 13233–13242, 2023.

[37] Tim Brooks, Ben Mildenhall, Tianfan Xue, Jiawen Chen, Dillon Sharlet, and Jonathan T Barron. Unprocessing images for learned raw denoising. In *Proceedings of the IEEE/CVF conference on computer vision and pattern recognition*, pages 11036–11045, 2019.

[38] Jiahong Fu, Qi Xie, Deyu Meng, and Zongben Xu. Rotation equivariant proximal operator for deep unfolding methods in image restoration. *IEEE Transactions on Pattern Analysis and Machine Intelligence*, 2024.

[39] Prasanna Sahoo and Thomas Riedel. *Mean value theorems and functional equations*. World Scientific, 1998.

A Theorem and Proofs

In this section, we present a comprehensive version of Theorem 1 and Proposition 1, which are briefly introduced in the main text, along with the related lemmas and proofs, aiming to provide a solid theoretical foundation for our proposed method.

It should be noted that we follow the previous works, and consider the equivariance on the orthogonal group $O(2)$[1]. Formally, $O(2) = \{A \in \mathbb{R}^{2\times 2} | A^T A = I_{2\times 2}\}$, which contains all rotation and reflection matrices. Without ambiguity, we use A to parameterize $O(2)$. We consider the Euclidean group $E(2) = \mathbb{R}^2 \rtimes O(2)$ ($\rtimes$ is a semidirect-product), whose element is represented as (x, A). Restricting the domain of A and x, we can also use this representation to parameterize any subgroup of $E(2)$. The input image can be modeled as a function defined on $\mathbb{R}^2$, denoted as $r(x)$. The intermediate feature map can be modeled as a function defined on $E(2)$, denoted as $e(x, A)$. We denote the function spaces of r and e as $C^\infty(\mathbb{R}^2)$ and $C^\infty(E(2))$, respectively.

A.1 Remark 1 and the Proof

Notations. For an input $r \in C^\infty(\mathbb{R}^2)$, transformations $\tilde{A} \in O(2)$ and $\tilde{b} \in \mathbb{R}^2$, $\tilde{A}$ acts on r by

$$f^R_{\tilde{A}\tilde{b}}[r](x) = r(\tilde{A}^{-1}(x - \tilde{b})), \forall x \in \mathbb{R}^2. \tag{14}$$

For a feature map $e \in C^\infty(E(2))$, $E(2) = \mathbb{R}^2 \ltimes O(2)$, and a transformation $\tilde{A} \in O(2)$, $\tilde{A}$ act on e by

$$f^E_{\tilde{A}\tilde{b}}[e](x, A, \tilde{b}) = e(\tilde{A}^{-1}(x - \tilde{b}), \tilde{A}^{-1}A), \forall (x, A) \in E(2). \tag{15}$$

Let Ψ denote the convolution on the input layer, which maps an input $r \in C^\infty(\mathbb{R}^2)$ to a feature map defined on $E(2)$:

$$\Psi[r](x, A) = \int_{\mathbb{R}^2} \varphi_{in}\left(A^{-1}\delta\right) r(x - \delta) d\sigma(\delta),\ \forall (x, A) \in E(2), \tag{16}$$

where σ is a measure on $\mathbb{R}^2$ and φ is the proposed parameterized filter. Φ denotes the convolution on the intermediate layer, which maps a feature map $e \in C^\infty(E(2))$ to another feature map defined on $E(2)$:

$$\Phi[e](x,B)=\int_{O(2)}\int_{\mathbb{R}^2}\varphi_A\left(B^{-1}\delta\right)e(x-\delta,BA)d\sigma(\delta)dv(A),\ \forall (x, B) \in E(2), \tag{17}$$

where v is a measure on $O(2)$, $A, B \in O(2)$ denote orthogonal transformations in the considered group, and $\varphi_{\tilde{A}}$ indicates the filter with respect to the channel of the feature map indexed by $\tilde{A}$, i.e., $e(x, A)|_{A=\tilde{A}}$. Υ denotes the convolution on the final layer, which maps a feature map $e \in C^\infty(E(2))$ to a function defined on $\mathbb{R}^2$:

$$\Upsilon[e](x)=\int_{O(2)}\int_{\mathbb{R}^2}\varphi_{out}\left(B^{-1}\delta\right) e(x-\delta, B)d\sigma(\delta)dv(B),\ \forall x \in \mathbb{R}^2. \tag{18}$$

Then we will prove Remark 1.

Remark 1. *For $r \in C^\infty(\mathbb{R}^2)$, $e \in C^\infty(E(2))$ and $\tilde{A} \in O(2)$, the following results are satisfied:*

$$\begin{aligned} \Psi\left[f^R_{\tilde{A}\tilde{b}}[r]\right] &= f^E_{\tilde{A}\tilde{b}}[\Psi[r]], \\ \Phi\left[f^E_{\tilde{A}\tilde{b}}[e]\right] &= f^E_{\tilde{A}\tilde{b}}[\Phi[e]], \\ \Upsilon\left[f^E_{\tilde{A}\tilde{b}}[e]\right] &= f^R_{\tilde{A}\tilde{b}}[\Upsilon[e]], \end{aligned} \tag{19}$$

where $f^R_{\tilde{A}\tilde{b}}$, $f^E_{\tilde{A}\tilde{b}}$, Ψ, Φ and Υ are defined by (14), (15), (16), (17) and (18), respectively.

[1]The rotation group S represents a subgroup of $O(2)$, and it is also regarded as the discretization of $O(2)$ in this paper.

Proof. (1) For any $x \in \mathbb{R}^2$, $A \in O(2)$, and $\tilde{b} \in \mathbb{R}^2$ we can obtain

$$
\begin{aligned}
&\Psi\left[f_{\tilde{A}\tilde{b}}^{R}[r]\right](x, A) \\
=&\int_{\mathbb{R}^2} \varphi_{in}\left(A^{-1}\delta\right) f_{\tilde{A}\tilde{b}}^{R}[r](x-\delta) d\sigma(\delta) \\
=&\int_{\mathbb{R}^2} \varphi_{in}\left(A^{-1}\delta\right) r(\tilde{A}^{-1}(x-\delta-\tilde{b})) d\sigma(\delta).
\end{aligned}
\tag{20}
$$

Let $\hat{\delta} = \tilde{A}^{-1}\delta$, since $|det(\tilde{A})| = 1$, and we have

$$
\begin{aligned}
&\int_{\mathbb{R}^2} \varphi_{in}\left(A^{-1}\delta\right) r(\tilde{A}^{-1}(x-\delta-\tilde{b})) d\sigma(\delta) \\
=&\int_{\mathbb{R}^2} \varphi_{in}\left(A^{-1}\tilde{A}\hat{\delta}\right) r(\tilde{A}^{-1}(x-\tilde{b})-\hat{\delta})) d\sigma(\hat{\delta}) \\
=&\int_{\mathbb{R}^2} \varphi_{in}\left((\tilde{A}^{-1}A)^{-1}\hat{\delta}\right) r(\tilde{A}^{-1}(x-\tilde{b})-\hat{\delta})) d\sigma(\hat{\delta}) \\
=&\Psi[r](\tilde{A}^{-1}(x-\tilde{b}), \tilde{A}^{-1}A) \\
=&f_{\tilde{A}\tilde{b}}^{E}[\Psi[r]](x, A, \tilde{b}).
\end{aligned}
\tag{21}
$$

This proves that $\Psi\left[f_{\tilde{A}\tilde{b}}^{R}[r]\right] = f_{\tilde{A}\tilde{b}}^{E}[\Psi[r]]$.

(2) Similar to the proof in (1), for any $x \in \mathbb{R}^2$, $B \in O(2)$, we can obtain

$$
\begin{aligned}
&\Phi\left[f_{\tilde{A}\tilde{b}}^{E}[e]\right](x, B) \\
=&\int_{\mathbb{R}^2}\int_{O(2)} \varphi_{A}\left(B^{-1}\delta\right) f_{\tilde{A}\tilde{b}}^{E}[e](x-\delta, BA, \tilde{b}) d\sigma(\delta) v(A) \\
=&\int_{\mathbb{R}^2}\int_{O(2)} \varphi_{A}\left(B^{-1}\delta\right) e(\tilde{A}^{-1}(x-\delta-\tilde{b}), \tilde{A}^{-1}BA) d\sigma(\delta) v(A) \\
=&\int_{\mathbb{R}^2}\int_{O(2)} \varphi_{A}\left(B^{-1}\tilde{A}\hat{\delta}\right) e(\tilde{A}^{-1}(x-\tilde{b})-\hat{\delta}, \tilde{A}^{-1}BA) d\sigma(\hat{\delta}) v(A) \\
=&\int_{\mathbb{R}^2}\int_{O(2)} \varphi_{A}\left((\tilde{A}^{-1}B)^{-1}\hat{\delta}\right) e(\tilde{A}^{-1}(x-\tilde{b})-\hat{\delta}, \tilde{A}^{-1}BA) d\sigma(\hat{\delta}) v(A) \\
=&\Phi[e](\tilde{A}^{-1}(x-\tilde{b}), \tilde{A}^{-1}B) \\
=&f_{\tilde{A}\tilde{b}}^{E}[\Phi[e]](x, B, \tilde{b}).
\end{aligned}
\tag{22}
$$

(3) For any $x \in \mathbb{R}^2$, we can deduce that

$$
\begin{aligned}
&\Upsilon\left[f_{\tilde{A}\tilde{b}}^{E}[e]\right](x) \\
=&\int_{\mathbb{R}^2}\int_{O(2)} \varphi_{out}\left(B^{-1}\delta\right) f_{\tilde{A}\tilde{b}}^{E}[e](x-\delta, B, \tilde{b}) d\sigma(\delta) v(B) \\
=&\int_{\mathbb{R}^2}\int_{O(2)} \varphi_{out}\left(B^{-1}\delta\right) e(\tilde{A}^{-1}(x-\delta-\tilde{b}), \tilde{A}^{-1}B) d\sigma(\delta) v(B) \\
=&\int_{\mathbb{R}^2}\int_{O(2)} \varphi_{out}\left(\left(\tilde{A}^{-1}B\right)^{-1}\hat{\delta}\right) e(\tilde{A}^{-1}(x-\tilde{b})-\hat{\delta}, \tilde{A}^{-1}B) d\sigma(\hat{\delta}) v(B). \\
=&\Upsilon[e](\tilde{A}^{-1}(x-\tilde{b})) \\
=&f_{\tilde{A}\tilde{b}}^{R}[\Upsilon[e]](x).
\end{aligned}
\tag{23}
$$

This proves that $\Upsilon\left[f_{\tilde{A}\tilde{b}}^{E}[e]\right] = f_{\tilde{A}\tilde{b}}^{R}[\Upsilon[e]]$. $\square$

A.2 Remark 2 and the Proof

Notations. We assume that an image $I \in R^{n\times n}$ represents a two-dimensional grid function obtained by discretizing a smooth function, i.e., for $i, j = 1, 2, \cdots, n$,

$$I_{ij} = r(\delta_{ij}), \tag{24}$$

where $\delta_{ij} = \left(\left(i - \frac{n+1}{2}\right)h, \left(j - \frac{n+1}{2}\right)h\right)^T$. We represent Z as a three-dimensional grid function sampled from a smooth function $e: \mathbb{R}^2 \times S \to \mathbb{R}$, i.e., for $i, j = 1, 2, \cdots, n$,

$$Z_{ij}^{A,\tilde{b}} = e(\delta_{ij}, A, \tilde{b}), \tag{25}$$

where $\delta_{ij} = \left(\left(i - \frac{n+1}{2}\right)h, \left(j - \frac{n+1}{2}\right)h\right)^T$ and $A \in S$, S is a subgroup of $O(2)$, and $\tilde{b} \in \mathbb{R}^2$ is translation. For $i, j = 1, 2, \cdots, p$, and $A, B \in S$, we have

$$\begin{aligned} \tilde{\Psi}_{ij}^{A} &= \varphi_{in}\left(A^{-1}\delta_{ij}\right), \\ \tilde{\Phi}_{ij}^{B,A} &= \varphi_{A}\left(B^{-1}\delta_{ij}\right), \\ \tilde{\Upsilon}_{ij}^{A} &= \varphi_{out}\left(A^{-1}\delta_{ij}\right), \end{aligned} \tag{26}$$

where $\delta_{ij} = ((i - {}^{(p+1)}/_2)\,h, (j - {}^{(p+1)}/_2)\,h)^T$, φ_{in}, φ_{out} and φ_A are parameterized filters. Let

$$\begin{aligned} \delta_{ij} &= \left(\left(i - \frac{p+1}{2}\right)h, \left(j - \frac{p+1}{2}\right)h\right)^T, \\ x_{ij} &= \left(\left(i - \frac{n+p+2}{2}\right)h, \left(j - \frac{n+p+2}{2}\right)h\right)^T. \end{aligned} \tag{27}$$

For $\forall A \in S$ and $i, j = 1, 2, \cdots, n$, the convolution of $\tilde{\Psi}$ and I is

$$\left(\tilde{\Psi} \star I\right)_{ij}^{A} = \sum_{(\tilde{i},\tilde{j})\in\Lambda} \varphi_{in}\left(A^{-1}\delta_{\tilde{i}\tilde{j}}\right) r\left(x_{ij} - \delta_{\tilde{i}\tilde{j}}\right), \tag{28}$$

where Λ is a set of indexes, denoted as $\Lambda = \{(i,j)|i,j = 1,2,\cdots,p\}$. For any $B \in S$ and $i, j = 1, 2, \cdots, n$, the convolution of $\tilde{\Phi}$ and Z is

$$\left(\tilde{\Phi} \star Z\right)_{ij}^{B} = \sum_{(\tilde{i},\tilde{j})\in\Lambda, A\in S} \varphi_{A}\left(B^{-1}\delta_{\tilde{i}\tilde{j}}\right) e\Big(x_{ij} - \delta_{\tilde{i}\tilde{j}}, BA\Big), \tag{29}$$

where $\Lambda = \{(i,j)|i,j = 1,2,\cdots,p\}$. For $i, j = 1, 2, \cdots, n$, the convolution of $\tilde{\Upsilon}$ and Z is

$$\left(\tilde{\Upsilon} \star Z\right)_{ij} = \sum_{(\tilde{i},\tilde{j})\in\Lambda, B\in S} \varphi_{out}\left(B^{-1}\delta_{\tilde{i}\tilde{j}}\right) e\Big(x_{ij} - \delta_{\tilde{i}\tilde{j}}, B\Big) \tag{30}$$

where $\Lambda = \{(i,j)|i,j = 1,2,\cdots,p\}$.

The transformations on I and Z are defined by

$$\begin{aligned} &\left(\tilde{f}_{\tilde{A}\tilde{b}}^{R}(I)\right)_{ij} = f_{\tilde{A}\tilde{b}}^{R}[r](x_{ij}), \left(\tilde{f}_{\tilde{A}\tilde{b}}^{\tilde{E}}(Z)\right)_{ij}^{A\tilde{b}} = f_{\tilde{A}\tilde{b}}^{E}[e](x_{ij}, A, \tilde{b}), \\ &\forall i, j = 1, 2, \cdots, n, \forall A, \tilde{A} \in S. \end{aligned} \tag{31}$$

Then we will prove the Remark 2. We firstly introduce the following necessary lemma.

Lemma 1. *For smooth functions $r: \mathbb{R}^2 \to \mathbb{R}$ and $\varphi: \mathbb{R}^2 \to \mathbb{R}$, if for $\delta \in \mathbb{R}^2$, the follow conditions are satisfied:*

$$\begin{aligned} &|r(\delta)| \le F_1, |\varphi(\delta)| \le F_2, \\ &\|\nabla r(\delta)\| \le G_1, \|\nabla \varphi(\delta)\| \le G_2, \\ &\|\nabla^2 r(\delta)\| \le H_1, \|\nabla^2 \varphi(\delta)\| \le H_2, \\ &\forall \|\delta\| \ge ({}^{p+1}/_2)h, \varphi(\delta) = 0, \end{aligned} \tag{32}$$

where $p, h > 0$, ∇ and ∇^2 denote the operators of gradient and Hessian matrix, respectively, then, $\forall \tilde{A} \in S, y \in \mathbb{R}$ the following results are satisfied:

$$\left| \int_{R^2} \varphi\left(\tilde{A}^{-1}\delta\right) r\left(x-\delta\right) d\sigma(\delta) - \sum_{i,j \in \Lambda} \varphi\left(\tilde{A}^{-1}\delta_{ij}\right) r\left(x-\delta_{ij}\right) h^2 \right| \leq \frac{(p+1)^2 C}{4} h^4, \tag{33}$$

where $\Lambda = \{(i,j)|i,j = 1,2,\cdots,p\}$, $\delta_{ij} = \left((i - {}^{(p+1)}/_2)\, h, (j - {}^{(p+1)}/_2)\, h\right)^T$ and $C = F_1H_2 + F_2H_1 + 2G_1G_2$.

The specific proof of lemma 1 can be referred to [11]. Based on lemma 1, let us prove Remark 2.

Remark 2. *Assume that an image $I \in \mathbb{R}^{n\times n}$ is discretized from the smooth function $r : \mathbb{R}^2 \to \mathbb{R}$ by (24), a feature map $Z \in \mathbb{R}^{n\times n\times t}$ is discretized from the smooth function $e : \mathbb{R}^2 \times S \to \mathbb{R}$ by (25), $|S| = t$, and filters $\tilde{\Psi}$, $\tilde{\Phi}$ and $\tilde{\Upsilon}$ are generated from φ_{in}, φ_{out} and $\varphi_A, \forall A \in S$, by (26), respectively. If for any $A \in S$, $x \in \mathbb{R}^2$, the following conditions are satisfied:*

$$\begin{aligned}
&|r(x)|, |e(x,A)| \leq F_1,\\
&\|\nabla r(x)\|, \|\nabla e(x,A)\| \leq G_1,\\
&\|\nabla^2 r(x)\|, \|\nabla^2 e(x,A)\| \leq H_1,\\
&|\varphi_{in}(x)|, |\varphi_A(x)|, |\varphi_{out}(x)| \leq F_2,\\
&\|\nabla\varphi_{in}(x)\|, \|\nabla\varphi_A(x)\|, \|\nabla\varphi_{out}(x)\| \leq G_2,\\
&\|\nabla^2\varphi_{in}(x)\|, \|\nabla^2\varphi_A(x)\|, \|\nabla^2\varphi_{out}(x)\| \leq H_2,\\
&\forall \|x\| \geq {}^{(p+1)h}/_2,\ \varphi_{in}(x), \varphi_A(x), \varphi_{out}(x) = 0,
\end{aligned} \tag{34}$$

where p is the filter size, h is the mesh size, and ∇ and ∇^2 denote the operators of gradient and Hessian matrix, respectively, then for any $\tilde{A} \in S$, the following results are satisfied:

$$\begin{aligned}
&\left\|\tilde{\Psi} \star \tilde{f}^{R}_{\tilde{A}\tilde{b}}(I) - \tilde{f}^{\tilde{E}}_{\tilde{A}\tilde{b}}\left(\tilde{\Psi} \star I\right)\right\|_\infty \leq \frac{C}{2}(p+1)^2h^2,\\
&\left\|\tilde{\Phi} \star \tilde{f}^{\tilde{E}}_{\tilde{A}\tilde{b}}(Z) - \tilde{f}^{\tilde{E}}_{\tilde{A}\tilde{b}}\left(\tilde{\Phi} \star Z\right)\right\|_\infty \leq \frac{C}{2}(p+1)^2h^2t,\\
&\left\|\tilde{\Upsilon} \star \tilde{f}^{\tilde{E}}_{\tilde{A}\tilde{b}}(Z) - \tilde{f}^{R}_{\tilde{A}\tilde{b}}\left(\tilde{\Upsilon} \star Z\right)\right\|_\infty \leq \frac{C}{2}(p+1)^2h^2t,
\end{aligned} \tag{35}$$

where $C = F_1H_2 + F_2H_1 + 2G_1G_2$, $\tilde{f}^{R}_{\tilde{A}\tilde{b}}$, $\tilde{f}^{\tilde{E}}_{\tilde{A}\tilde{b}}$, $\tilde{\Psi}$, $\tilde{\Phi}$ and $\tilde{\Upsilon}$ are defined by (26) and (31), respectively. The operators $\star$ involved in Eq. (35) are defined in (28), (29) and (30), respectively, and $\|\cdot\|_\infty$ represents the infinity norm.

Proof. For any $x \in \mathbb{R}, A, B \in S$, let

$$\hat{\Psi}[r](x,A) = \sum_{(\tilde{i},\tilde{j})\in\Lambda} \varphi_{in}\left(A^{-1}\delta_{\tilde{i}\tilde{j}}\right) r\left(x - \delta_{\tilde{i}\tilde{j}}\right), \tag{36}$$

where $\Lambda = \{(\tilde{i},\tilde{j})|\tilde{i},\tilde{j} = 1,2,\cdots,p\}$. Then, for any $A \in S$, we can obtain

$$\hat{\Psi}[r](x_{ij},A) = \left(\tilde{\Psi} \star I\right)^A_{ij}. \tag{37}$$

1) By **Remark 1**, we know that $\Psi\left[f^{R}_{\tilde{A}\tilde{b}}[r]\right] = f^{E}_{\tilde{A}\tilde{b}}\left[\Psi[r]\right]$. Thus for any $A \in S$, we have

$$\begin{aligned}
&\left|\left(\tilde{\Psi} \star \tilde{f}^{R}_{\tilde{A}\tilde{b}}(I) - \tilde{f}^{\tilde{E}}_{\tilde{A}\tilde{b}}\left(\tilde{\Psi} \star I\right)\right)^A_{ij}\right|\\
=&\left|\hat{\Psi}\left[f^{R}_{\tilde{A}\tilde{b}}[r]\right](x_{ij},A) - f^{E}_{\tilde{A}\tilde{b}}\left[\hat{\Psi}[r]\right](x_{ij},A)\right|\\
\leq&\left|\hat{\Psi}\left[f^{R}_{\tilde{A}\tilde{b}}[r]\right](x_{ij},A) - \frac{1}{h^2}\Psi\left[f^{R}_{\tilde{A}\tilde{b}}[r]\right](x_{ij},A)\right|\\
+&\left|f^{E}_{\tilde{A}\tilde{b}}\left[\hat{\Psi}[r]\right](x_{ij},A) - \frac{1}{h^2}f^{E}_{\tilde{A}\tilde{b}}\left[\Psi[r]\right](x_{ij},A)\right|.
\end{aligned} \tag{38}$$

Let $\hat{r}=f^{R}_{\tilde{A}\tilde{b}}[r]$, and then it is easy to deduce that $\hat{r}$ satisfies the conditions in **lemma 1**. Then, by **lemma 1**,

$$\begin{aligned}
&\left|\hat{\Psi}\left[f^{R}_{\tilde{A}\tilde{b}}[r]\right](x_{ij},A)-\frac{1}{h^2}\Psi\left[f^{R}_{\tilde{A}\tilde{b}}[r]\right](x_{ij},A)\right|\\
=&\frac{1}{h^2}\left|\hat{\Psi}\left[f^{R}_{\tilde{A}\tilde{b}}[r]\right](x_{ij},A)h^2-\Psi\left[f^{R}_{\tilde{A}\tilde{b}}[r]\right](x_{ij},A)\right|\\
=&\frac{1}{h^2}\left|\sum_{(i,j)\in\Lambda}\varphi_{in}\left(A^{-1}\delta_{ij}\right)\hat{r}\left(x_{ij}-\delta_{ij}\right)h^2-\int_{\mathbb{R}^2}\varphi_{in}\left(A^{-1}\delta\right)\hat{r}(x_{ij}-\delta)d\sigma(\delta)\right|\\
\leq&\frac{(p+1)^2C}{4}h^2.
\end{aligned}\tag{39}$$

Besides, let $\hat{A}=\tilde{A}^{-1}A$ and $\hat{x}_{ij}=\tilde{A}^{-1}(x_{ij}-\tilde{b})$, and by **lemma 1**, we can also achieve,

$$\begin{aligned}
&\left|f^{E}_{\tilde{A}\tilde{b}}\left[\hat{\Psi}[r]\right](x_{ij},A)-\frac{1}{h^2}f^{E}_{\tilde{A}\tilde{b}}\left[\Psi[r]\right](x_{ij},A)\right|\\
=&\frac{1}{h^2}\left|f^{E}_{\tilde{A}\tilde{b}}\left[\hat{\Psi}[r]\right](x_{ij},A)h^2-f^{E}_{\tilde{A}\tilde{b}}\left[\Psi[r]\right](x_{ij},A)\right|\\
=&\frac{1}{h^2}\left|\left[\hat{\Psi}[r]\right](\tilde{A}^{-1}(x_{ij}-\tilde{b}),\tilde{A}^{-1}A)h^2-\left[\Psi[r]\right](\tilde{A}^{-1}(x_{ij}-\tilde{b}),\tilde{A}^{-1}A)\right|\\
=&\frac{1}{h^2}\left|\sum_{(i,j)\in\Lambda}\varphi_{in}\left(A^{-1}\tilde{A}\delta_{ij}\right)r\left(\tilde{A}^{-1}(x_{ij}-\tilde{b})-\delta_{ij}\right)h^2-\int_{\mathbb{R}^2}\varphi_{in}\left(A^{-1}\tilde{A}\delta\right)r(\tilde{A}^{-1}(x_{ij}-\tilde{b})-\delta)d\sigma(\delta)\right|\\
=&\frac{1}{h^2}\left|\sum_{(i,j)\in\Lambda}\varphi_{in}\left(\hat{A}^{-1}\delta_{ij}\right)r\left(\hat{x}_{ij}-\delta_{ij}\right)h^2-\int_{\mathbb{R}^2}\varphi_{in}\left(\hat{A}^{-1}\delta\right)r(\hat{x}_{ij}-\delta)d\sigma(\delta)\right|\\
\leq&\frac{(p+1)^2C}{4}h^2.
\end{aligned}\tag{40}$$

Thus, combining (38), (39) and (40), we can achieve

$$\left|\hat{\Psi}\left[f^{R}_{\tilde{A}\tilde{b}}[r]\right](x_{ij},A,\tilde{b})-f^{E}_{\tilde{A}\tilde{b}}\left[\hat{\Psi}[r]\right](x_{ij},A,\tilde{b})\right|\leq\frac{C}{2}(p+1)^2h^2.\tag{41}$$

In other word,

$$\left|\left(\tilde{\Psi}\star\tilde{f}^{R}_{\tilde{A}\tilde{b}}(I)-\tilde{f}^{\tilde{E}}_{\tilde{A}\tilde{b}}\left(\tilde{\Psi}\star I\right)\right)^{A}_{ij}\right|\leq\frac{C}{2}(p+1)^2h^2.\tag{42}$$

This proves the first inequality in (35).

2) For any $A,B\in S$, let $\hat{B}=\tilde{A}^{-1}B$, $r_A(x)=e(x,A)$, and $\hat{\Psi}_A$ be a operator defined in the formulation of (36), while correlated to φ_A. Then, for any $i,j=1,2,\cdots,n$, $B\in S$,

$$\begin{aligned}
&\left|\left(\tilde{\Phi}\star\tilde{f}^{\tilde{E}}_{\tilde{A}\tilde{b}}(Z)-\tilde{f}^{\tilde{E}}_{\tilde{A}\tilde{b}}\left(\tilde{\Phi}\star Z\right)\right)^{B}_{ij}\right|\\
=&\left|\sum_{(\tilde{i},\tilde{j})\in\Lambda,A\in S}\varphi_A\left(B^{-1}\delta_{\tilde{i}\tilde{j}}\right)e\left(\tilde{A}^{-1}\left(x_{ij}-\delta_{\tilde{i}\tilde{j}}-\tilde{b}\right),\tilde{A}^{-1}BA\right)-\sum_{(\tilde{i},\tilde{j})\in\Lambda,A\in S}\varphi_A\left(B^{-1}\tilde{A}\delta_{\tilde{i}\tilde{j}}\right)e\left(\tilde{A}^{-1}(x_{ij}-\tilde{b})-\delta_{\tilde{i}\tilde{j}},\tilde{A}^{-1}BA\right)\right|\\
\leq&\sum_{A\in S}\left|\sum_{(\tilde{i},\tilde{j})\in\Lambda}\varphi_A\left(B^{-1}\delta_{\tilde{i}\tilde{j}}\right)r_{\hat{B}A}\left(\tilde{A}^{-1}(x_{ij}-\delta_{\tilde{i}\tilde{j}}-\tilde{b})\right)-\sum_{(\tilde{i},\tilde{j})\in\Lambda}\varphi_A\left(B^{-1}\tilde{A}\delta_{\tilde{i}\tilde{j}}\right)r_{\hat{B}A}\left(\tilde{A}^{-1}(x_{ij}-\tilde{b})-\delta_{\tilde{i}\tilde{j}}\right)\right|\\
=&\sum_{A\in S}\left|\sum_{(\tilde{i},\tilde{j})\in\Lambda}\varphi_A\left(B^{-1}\delta_{\tilde{i}\tilde{j}}\right)f^{R}_{\tilde{A}\tilde{b}}[r_{\hat{B}A}]\left(x_{ij}-\delta_{\tilde{i}\tilde{j}}\right)-\sum_{(\tilde{i},\tilde{j})\in\Lambda}\varphi_A\left(B^{-1}\tilde{A}\delta_{\tilde{i}\tilde{j}}\right)r_{\hat{B}A}\left(\tilde{A}^{-1}(x_{ij}-\tilde{b})-\delta_{\tilde{i}\tilde{j}}\right)\right|\\
=&\sum_{A\in S}\left|\hat{\Psi}_A\left[f^{R}_{\tilde{A}\tilde{b}}[r_{\hat{B}A}]\right](x_{ij},B,\tilde{b})-f^{E}_{\tilde{A}\tilde{b}}\left[\hat{\Psi}_A[r_{\hat{B}A}]\right](x_{ij},B,\tilde{b})\right|.
\end{aligned}$$

Then by (41), we can achieve that $\forall i, j = 1, 2, \cdots, n$, $B \in S$,

$$\left|\left(\tilde{\Phi} \star \tilde{f}^{\tilde{E}}_{\tilde{A}\tilde{b}}(Z) - \tilde{f}^{\tilde{E}}_{\tilde{A}\tilde{b}}\left(\tilde{\Phi} \star Z\right)\right)^{B}_{ij}\right| \leq \frac{C}{2}(p+1)^2 h^2 t. \tag{43}$$

This proves the second inequality in (35).

3) For any $A, B \in S$, let $\hat{B} = \tilde{A}^{-1}B$, $r_A(x) = e(x, A)$, and $\hat{\Psi}_{out}$ be a operator defined in the formulation of (36), while correlated to φ_{out}.

Then, we have that $\forall i, j = 1, 2, \cdots, n$,

$$\begin{aligned}
&\left|\left(\tilde{\Upsilon} \star \tilde{f}^{\tilde{E}}_{\tilde{A}\tilde{b}}(Z) - \tilde{f}^{\tilde{E}}_{\tilde{A}\tilde{b}}\left(\tilde{\Upsilon} \star Z\right)\right)_{ij}\right| \\
=& \left|\sum_{(\tilde{i},\tilde{j})\in\Lambda, B\in S} \varphi_{out}\left(B^{-1}\delta_{\tilde{i}\tilde{j}}\right) e\left(\tilde{A}^{-1}\left(x_{ij} - \delta_{\tilde{i}\tilde{j}} - \tilde{b}\right), \tilde{A}^{-1}B\right) - \sum_{(\tilde{i},\tilde{j})\in\Lambda, B\in S} \varphi_{out}\left(B^{-1}\tilde{A}\delta_{\tilde{i}\tilde{j}}\right) e\left(\tilde{A}^{-1}(x_{ij} - \tilde{b}) - \delta_{\tilde{i}\tilde{j}}, \tilde{A}^{-1}B\right)\right| \\
\leq& \sum_{B\in S}\left|\sum_{(\tilde{i},\tilde{j})\in\Lambda} \varphi_{out}\left(B^{-1}\delta_{\tilde{i}\tilde{j}}\right) r_{\hat{B}}\left(\tilde{A}^{-1}\left(x_{ij} - \delta_{\tilde{i}\tilde{j}} - \tilde{b}\right)\right) - \sum_{(\tilde{i},\tilde{j})\in\Lambda} \varphi_{out}\left(B^{-1}\tilde{A}\delta_{\tilde{i}\tilde{j}}\right) r_{\hat{B}}\left(\tilde{A}^{-1}(x_{ij} - \tilde{b}) - \delta_{\tilde{i}\tilde{j}}\right)\right| \\
=& \sum_{B\in S}\left|\sum_{(\tilde{i},\tilde{j})\in\Lambda} \varphi_{out}\left(B^{-1}\delta_{\tilde{i}\tilde{j}}\right) f^{R}_{\tilde{A}\tilde{b}}[r_{\hat{B}}]\left(x_{ij} - \delta_{\tilde{i}\tilde{j}}\right) - \sum_{(\tilde{i},\tilde{j})\in\Lambda} \varphi_{out}\left(B^{-1}\tilde{A}\delta_{\tilde{i}\tilde{j}}\right) r_{\hat{B}}\left(\tilde{A}^{-1}(x_{ij} - \tilde{b}) - \delta_{\tilde{i}\tilde{j}}\right)\right| \\
=& \sum_{B\in S}\left|\hat{\Psi}_{out}\left[f^{R}_{\tilde{A}\tilde{b}}[r_{\hat{B}}]\right](x_{ij}, B, \tilde{b}) - f^{E}_{\tilde{A}\tilde{b}}\left[\hat{\Psi}_{out}[r_{\hat{B}}]\right](x_{ij}, B, \tilde{b})\right|.
\end{aligned}$$

Then by (41), we can achieve that $\forall i, j = 1, 2, \cdots, n$,

$$\left|\left(\tilde{\Upsilon} \star \tilde{f}^{\tilde{E}}_{\tilde{A}\tilde{b}}(Z) - \tilde{f}^{\tilde{E}}_{\tilde{A}\tilde{b}}\left(\tilde{\Upsilon} \star Z\right)\right)_{ij}\right| \leq \frac{C}{2}(p+1)^2 h^2 t. \tag{44}$$

This proves the third inequality in (35).

□

A.3 Theorem 1 and the Proof

Notations. In the following, we provide the corresponding formulations, just like [11, 38]. It should be noted that for convenience in subsequent proofs, $|A| \leq a$ indicates that all elements of A are less than a, and $|A| \leq |B|$ implies that the value of any element a_{ij} at position (i, j) in A is less than the value of the corresponding element b_{ij} in B.

For an input $r \in C^{\infty}(\mathbb{R}^2)$, translation $b \in \mathbb{R}^2$ and a degree $\theta \in [0, 2\pi]$, $A_\theta \in O(2)$ is the rotation matrix $\begin{bmatrix} \cos\theta, -\sin\theta \\ \sin\theta, \cos\theta \end{bmatrix}$. A_θ acts on r by

$$f^{R}_{\theta b}[r](x) = r(A_\theta^{-1}(x - b)), \forall x \in \mathbb{R}^2. \tag{45}$$

For a feature map $e \in C^{\infty}(E(2))$, $E(2) = \mathbb{R}^2 \ltimes O(2)$, and a degree $\theta \in [0, 2\pi]$. A_θ acts on e by

$$f^{E}_{\theta b}[e](x, A, b) = e(A_\theta^{-1}(x - b), A_\theta^{-1}A), \forall (x, A, b) \in E(2). \tag{46}$$

Considering an multi-channel image $I \in \mathbb{R}^{H\times W\times C}$ as input, which can be naturally represented by a two-dimensional grid function. Suppose the filter is of size $p \times p$, then, the mesh grids for filter and image can be respectively represented as follows:

$$\delta_{kl} = \left(\left(k - \frac{p+1}{2}\right)h, \left(l - \frac{p+1}{2}\right)h\right)^T, \; x_{kl} = \left(\left(k - \frac{H+1}{2}\right)h, \left(l - \frac{W+1}{2}\right)h\right)^T. \tag{47}$$

Then, each channel of I can be obtained by discretizing a smooth function, i.e., for $k = 1, 2, \cdots, W$, $l = 1, 2, \cdots, H$, and $c = 1, 2, \cdots, C$,

$$I_{kl}^{c} = r_c(x_{kl}), \tag{48}$$

where r_c is latent function for the c^{th} channel.

We denote the equivariant number as t and the correlated rotation group of the equivariant convolution as S, respectively. Then, $|S| = t$ and $S = \{A_\theta | \theta = {}^{2\pi k}/_{t}, k = 1, 2, \cdots, t\}$. We represent the feature map of equivariant convolution as $Z \in \mathbb{R}^{H \times W \times t \times C}$. Z is a four-dimensional grid function, whose c^{th} channel is sampled from a smooth function $e_c : \mathbb{R}^2 \times S \to \mathbb{R}$, i.e., for $k = 1, 2, \cdots, W$ and $l = 1, 2, \cdots, H$,

$$Z_{kl}^{A,c} = e_c(x_{kl}, A), \tag{49}$$

where $A \in S$.

Input layer. The filter of the input multi-channel convolution layer can be represented as

$$\tilde{\Psi}_{kl}^{A,c,d} = \varphi_{cd}\left(A^{-1}\delta_{kl}\right), \tag{50}$$

where φ_{cd} is the parameterized filter, $A \in S$, $c = 1, 2, \cdots, n_c$, $d = 1, 2, \cdots, n_d$, n_c and n_d are the input and output channel numbers, respectively. Denoting multi-channel convolution of $\tilde{\Psi}$ and I in the input layer as $Z = \hat{\Psi}(I)$, then it can be calculated by

$$\hat{\Psi}(I)^{A,d} = \sum_{c} \tilde{\Psi}^{A,c,d} * I^{c}, \tag{51}$$

where $*$ denotes the 2-D convolution operation. It can be also rewritten in the following more detailed formulation:

$$\hat{e}_d(x_{kl}, A) = \sum_{c,\delta \in \Lambda} \varphi_{cd}\left(A^{-1}\delta\right) r_c\left(x_{kl} - \delta\right), \tag{52}$$

where Λ is a set of indexes, denoted as $\Lambda = \{\delta_{\hat{k}\hat{l}} | \hat{k}, \hat{l} = 1, 2, \cdots, p\}$, $A \in S$, $k = 1, 2, \cdots, W$ and $l = 1, 2, \cdots, H$.

Intermediate layer. The filter of the intermediate multi-channel convolution layer can be represented as

$$\tilde{\Phi}_{kl}^{A,B,c,d} = \varphi_{Acd}\left(B^{-1}\delta_{kl}\right), \tag{53}$$

where φ_{Acd} is the parameterized filter, $A, B \in S$, $c = 1, 2, \cdots, n_c$, $d = 1, 2, \cdots, n_d$, n_c and n_d are the input and output channel numbers, respectively. Denoting the multi-channel convolution of $\tilde{\Phi}$ and Z in the intermediate layer as $\hat{Z} = \hat{\Phi}(Z)$, then it can be calculated by

$$\hat{\Phi}(Z)^{B,d} = \sum_{c,A} \tilde{\Phi}^{A,B,c,d} * Z^{A,c}. \tag{54}$$

It can also be rewritten in the following more detailed formulation:

$$\hat{e}_d(x_{kl}, B) = \sum_{c,A,\delta \in \Lambda} \varphi_{Acd}\left(B^{-1}\delta\right) e_c\left(x_{kl} - \delta, BA\right). \tag{55}$$

Output layer. The filter of the output multi-channel convolution layer can be represented as

$$\tilde{\Upsilon}_{kl}^{B,c,d} = \varphi_{cd}\left(B^{-1}\delta_{kl}\right), \tag{56}$$

where φ_{cd} is the parameterized filter, $B \in S$, $c = 1, 2, \cdots, n_c$, $d = 1, 2, \cdots, n_d$, n_c and n_d are the input and output channel numbers, respectively. Denoting the multi-channel convolution of $\tilde{\Upsilon}$ and Z in the output layer as $\hat{Y} = \hat{\Upsilon}(Z)$, then it can be calculated by

$$\hat{\Upsilon}(Z)^{d} = \sum_{c,B} \tilde{\Upsilon}^{B,c,d} * Z^{B,c}. \tag{57}$$

It can be also rewritten in the following more detailed formulation:

$$\hat{r}_d(x_{kl}) = \sum_{c,B,\delta \in \Lambda} \varphi_{cd}\left(B^{-1}\delta\right) e_c\left(x_{kl} - \delta, B\right). \tag{58}$$

The transformations on each channel of the input image and the feature map are defined by

$$
\begin{gathered}
\left(\tilde{f}^R_{\theta b}(I)\right)^c_{kl} = f^R_{\theta b}[r_c](x_{kl}),\ \left(\tilde{f}^{\tilde{E}}_{\theta b}(Z)\right)^{A,c}_{kl} = f^E_{\theta b}[e_c](x_{kl}, A, b), \\
\forall k = 1, 2, \cdots, H, l = 1, 2, \cdots, W, c = 1, 2, \cdots, C, \forall A \in S, \theta \in [0, 2\pi].
\end{gathered}
\tag{59}
$$

For expression conciseness we further denote

$$
\tilde{f}_{\theta b}[x] = \begin{cases} \tilde{f}^R_{\theta b}[x] & \text{if} \quad \forall x \in \mathbb{R}^{H\times W\times C} \\ \tilde{f}^{\tilde{E}}_{\theta b}[x] & \text{if} \quad \forall x \in \mathbb{R}^{H\times W\times t\times C} \end{cases}. \tag{60}
$$

Following the [38], for a feature map $Z \in \mathbb{R}^{H\times W\times t\times C}$, we say the channel number of the correlated convolution layer is tC, due to the fact that Z is usually reshaped into the shape of $H \times W \times tC$ for implementation convenience, and the flop of the correlated equivariant convolution layer is similar to a tC-channel convolution layer.

Then we will prove the Theorem 1. Before this, we first present the following necessary lemmas and the specific proof can be referred to [38].

Lemma 2. *For an image I with size $H \times W \times n_0$, and a N-layer rotation equivariant CNN network* $\mathrm{g}(\cdot)$, *whose channel number of the i^{th} layer is n_i, rotation equivariant subgroup is $S \leqslant O(2)$, $|S| = t$, and activation function is set as ReLU. If the latent continuous function of the c^{th} channel of I denoted as $r_c : \mathbb{R}^2 \to \mathbb{R}$, and the latent continuous function of any convolution filters in the i^{th} layer denoted as $\varphi^i : \mathbb{R}^2 \to \mathbb{R}$, where $i \in \{1, \cdots, N\}$, $c \in \{1, \cdots, n_0\}$, for any $x \in \mathbb{R}^2$, the following conditions are satisfied:*

$$
\begin{aligned}
&|r_c(x)| \leq F_0, \|\nabla r_c(x)\| \leq G_0, \|\nabla^2 r_c(x)\| \leq H_0, \\
&|\varphi^i(x)| \leq F_i, \|\nabla \varphi^i(x)\| \leq G_i, \|\nabla^2 \varphi^i(x)\| \leq H_i, \\
&\forall \|x\| \geq {}^{(p+1)h}/_2,\ \varphi_i(x) = 0,
\end{aligned}
\tag{61}
$$

where p is the filter size, h is the mesh size, and ∇ and ∇^2 denote the operators of gradient and Hessian matrix, respectively. Denote

$$
e^i_d(x, B) = \begin{cases} \sum_{c,\delta\in\Lambda} \varphi^1_{cd}(B^{-1}\delta) r_c(x - \delta) & \text{if} \quad i = 1, \\ \sum_{c,A,\delta\in\Lambda} \varphi^i_{Acd}(B^{-1}\delta) e^{i-1}_c(x - \delta, BA) & \text{if} \quad i \neq 1, N \end{cases} \tag{62}
$$

where $\Lambda = \left\{\left(\left(k - \frac{p+1}{2}\right)h, \left(l - \frac{p+1}{2}\right)h\right)^T | k, l = 1, 2, \cdots, p\right\}$, φ^1_{cd} and φ^i_{Acd} are filters in the first layer and other layers respectively. Then, for $\forall B \in S$ the following results are satisfied:

$$
\left|e^i_d(x, B)\right| \leq F_0 \mathcal{F}_i, \tag{63}
$$

$$
\left|\nabla e^i_d(x, B)\right| \leq \left(\sum_{m=1}^{i} \frac{G_m F_0}{F_m} + G_0\right) \mathcal{F}_i, \tag{64}
$$

$$
\left|\nabla^2 e^i_d(x, B)\right| \leq \left(\sum_{m=1}^{i} \frac{H_m F_0}{F_m} + 2\sum_{l=1}^{i} \frac{G_l}{F_l} \sum_{m=1}^{l-1} \frac{G_m F_0}{F_m} + 2\sum_{m=1}^{i} \frac{G_m G_0}{F_m} + H_0\right) \mathcal{F}_i, \tag{65}
$$

where $\mathcal{F}_i = \prod_{k=1}^{i} n_{k-1} p^2 F_k$, $\forall i = 1, 2, \cdots, N-1$.

Lemma 3. *For an image I with size $H \times W \times n_0$, and a N-layer rotation equivariant CNN network* $\mathrm{g}(\cdot)$, *whose channel number of the i^{th} layer is n_i, rotation equivariant subgroup is $S \leqslant O(2)$, $|S| = t$, and activation function is set as ReLU. If the latent continuous function of the c^{th} channel of I denoted as $r_c : \mathbb{R}^2 \to \mathbb{R}$, and the latent continuous function of any convolution filters in the i^{th} layer denoted as $\varphi^i : \mathbb{R}^2 \to \mathbb{R}$, where $i \in \{1, \cdots, N\}$, $c \in \{1, \cdots, n_0\}$, for any $x \in \mathbb{R}^2$, the following conditions are satisfied:*

$$
\begin{aligned}
&|r_c(x)| \leq F_0, \|\nabla r_c(x)\| \leq G_0, \|\nabla^2 r_c(x)\| \leq H_0, \\
&|\varphi^i(x)| \leq F_i, \|\nabla \varphi^i(x)\| \leq G_i, \|\nabla^2 \varphi^i(x)\| \leq H_i, \\
&\forall \|x\| \geq {}^{(p+1)h}/_2,\ \varphi_i(x) = 0,
\end{aligned}
\tag{66}
$$

where p is the filter size, h is the mesh size, ∇ and ∇^2 denote the operators of gradient and Hessian matrix, respectively. For an arbitrary $\theta \in [0, 2\pi]$, A_θ denotes the rotation matrix. If $F(\theta) = \mathrm{g}\left[\tilde{f}_{\theta b}\right](I) = \hat{\Upsilon}\left[\hat{\Phi}_{N-1} \cdots \hat{\Phi}_{i+1}\left[\hat{\Phi}_i \cdots \hat{\Phi}_2\left[\hat{\Psi}\left[\tilde{f}_{\theta b}\right]\right] \cdots\right]\right](I)$, then the following result is satisfied:

$$|F'(\theta)| \leq \mathcal{F}\left(\max\{H, W\} + N(p+1)\right) hG_0, \tag{67}$$

where $\mathcal{F} = \prod_{k=1}^{N} n_{k-1} p^2 F_k$.

Lemma 4. *Under the same conditions with lemma 3,*
If $F(\theta) = \tilde{f}_{\theta b}[\mathrm{g}](I) = \tilde{f}_{\theta b}\left[\hat{\Upsilon}\left[\hat{\Phi}_{N-1} \cdots \hat{\Phi}_{i+1}\left[\hat{\Phi}_i \cdots \hat{\Phi}_2\left[\hat{\Psi}\right] \cdots\right]\right]\right](I)$, and then the following result is satisfied:

$$|F'(\theta)| \leq \mathcal{F} \max\{H, W\} hG_0, \tag{68}$$

where $\mathcal{F} = \prod_{k=1}^{N} n_{k-1} p^2 F_k$.

Then, let us give Theorem 1 and prove it based on the aforementioned Lemmas.

Theorem 1. *For an image I with size $H \times W \times n_0$, and a N-layer rotation-translation equivariant CNN network $\mathrm{g}(\cdot)$, whose channel number of the i^{th} layer is n_i, rotation equivariant subgroup is $S \leqslant O(2)$, $|S| = t$, and activation function is set as ReLU. If the latent continuous function of the c^{th} channel of I denoted as $r_c : \mathbb{R}^2 \to \mathbb{R}$, and the latent continuous function of any convolution filters in the i^{th} layer denoted as $\varphi^i : \mathbb{R}^2 \to \mathbb{R}$, where $i \in \{1, \cdots, N\}$, $c \in \{1, \cdots, n_0\}$, for any $x \in \mathbb{R}^2$, the following conditions are satisfied:*

$$\begin{aligned} &|r_c(x)| \leq F_0, \|\nabla r_c(x)\| \leq G_0, \|\nabla^2 r_c(x)\| \leq H_0, \\ &|\varphi^i(x)| \leq F_i, \|\nabla \varphi^i(x)\| \leq G_i, \|\nabla^2 \varphi^i(x)\| \leq H_i, \\ &\forall \|x\| \geq {}^{(p+1)h}/_2,\ \varphi_i(x) = 0, \end{aligned} \tag{69}$$

where p is the filter size, h is the mesh size, ∇ and ∇^2 denote the operators of gradient and Hessian matrix, respectively. For an arbitrary $0 \leq \theta \leq 2\pi$, $A_\theta \in S$ denotes the rotation matrix, $b \in \mathbb{R}^2$ denotes the translation, and the following result is satisfied:

$$\left\| \tilde{f}_{\theta b}^{-1}\, \mathrm{g}\left[\tilde{f}_{\theta b}\right](I) - [\mathrm{g}]\,(I) \right\|_\infty \leq C_1 h^2 + C_2 p h t^{-1}, \tag{70}$$

where $\tilde{f}_{\theta b}$ is defined in Eq. (60) and

$$\begin{aligned} C_1 &= 2N\mathcal{F} \cdot \sum_{i=1}^{N}\left(\frac{H_i F_0}{F_i} + 2\frac{G_i}{F_i}\sum_{m=1}^{i-1}\frac{G_m F_0}{F_m} + 2\frac{G_i G_0}{F_i} + H_0\right), \\ C_2 &= 2\pi G_0 \mathcal{F}\left(2\max\{H,W\}p^{-1} + 2N\right), \mathcal{F} = \prod\nolimits_{i=1}^{N} n_{i-1} p^2 F_i. \end{aligned} \tag{71}$$

Proof. Let $\hat{I} = \tilde{f}_{\theta b} I$, we can split the left part of Eq. (70) as

$$\begin{aligned} &\left| \tilde{f}_{\theta b}^{-1}\, \mathrm{g}\left[\tilde{f}_{\theta b}\right](I) - [\mathrm{g}](I) \right| \\ =& \left| \tilde{f}_{\theta b}^{-1}\, \mathrm{g}(\hat{I}) - \mathrm{g}\left[\tilde{f}_{\theta b}^{-1}\right](\hat{I}) \right| \\ \leq& \underbrace{\left| \mathrm{g}\left[\tilde{f}_{\theta b}^{-1}\right](\hat{I}) - \mathrm{g}\left[\tilde{f}_{\theta_k b}^{-1}\right](\hat{I}) \right|}_{\langle 1 \rangle} + \underbrace{\left| \mathrm{g}\left[\tilde{f}_{\theta_k b}^{-1}\right](\hat{I}) - \tilde{f}_{\theta_k b}^{-1}\,[\mathrm{g}]\,(\hat{I}) \right|}_{\langle 2 \rangle} + \underbrace{\left| \tilde{f}_{\theta_k b}^{-1}\,[\mathrm{g}](\hat{I}) - \tilde{f}_{\theta b}^{-1}\,[\mathrm{g}](\hat{I}) \right|}_{\langle 3 \rangle}, \end{aligned} \tag{72}$$

where $\theta = \theta_k + \delta$, where $k = 1, 2, \cdots, t$, $0 \leq \delta \leq {}^{2\pi}/_t$. Next, we need to estimate the error bounds of the above three items, separately. It should be noted that the following proof is deduced without the ReLU activation function for concise. However, the conclusions are all still correct for networks with the ReLU activation function, since ReLU does not disturb the equivariance or amplify the error bound.

Firstly, we prove the following inequality for the part $\langle 1 \rangle$ of Eq. (72).

$$\left| \mathrm{g}\left[\tilde{f}_{\theta b}^{-1}\right](\hat{I}) - \mathrm{g}\left[\tilde{f}_{\theta_k b}^{-1}\right](\hat{I})\right| \leq \frac{2\pi}{t}\mathcal{F}\left(\max\left\{H,W\right\} + N\left(p+1\right)\right)hG_0. \tag{73}$$

Let us denote $F_1(\theta) = \mathrm{g}\left[\tilde{f}_{\theta b}\right](\hat{I})$. Obviously the function $F_1(\theta)$ is continuous with respect to θ, so we have the following conclusion by the Lagrange Mean Value Theorem [39]

$$\begin{aligned} \left| \mathrm{g}\left[\tilde{f}_{\theta b}\right](\hat{I}) - \mathrm{g}\left[\tilde{f}_{\theta_k b}\right](\hat{I})\right| &= \left|F_1(\theta) - F_1(\theta_k)\right| \\ &\leq \left|F_1'(\xi_1)\right|\delta \\ &\leq \frac{2\pi}{t}\left|F_1'(\xi_1)\right|, \end{aligned} \tag{74}$$

where $0 < \xi_1 < \delta$ and by lemma 3 we have $|F_1'(\xi_1)| \leq \mathcal{F}\left(\max\left\{H,W\right\} + N\left(p+1\right)\right)hG_0$. Then we can prove Eq. (73).

Secondly, we prove the following inequality for the part $\langle 3 \rangle$ of Eq. (72).

$$\left| \tilde{f}_{\theta_k b}\left[\mathrm{g}\right](\hat{I}) - \tilde{f}_{\theta b}\left[\mathrm{g}\right](\hat{I})\right| \leq \frac{2\pi}{t}\mathcal{F}\max\left\{H,W\right\}hG_0. \tag{75}$$

Let us denote $F_2(\theta) = \tilde{f}_{\theta b}\left[\mathrm{g}\right](\hat{I})$. Obviously the function $F_2(\theta)$ is continuous with respect to θ, so we have the following conclusion by the Lagrange Mean Value Theorem [39]

$$\begin{aligned} \left| \tilde{f}_{\theta_k b}\left[\mathrm{g}\right](\hat{I}) - \tilde{f}_{\theta b}\left[\mathrm{g}\right](\hat{I})\right| &= \left|F_2(\theta) - F_2(\theta_k)\right| \\ &\leq \left|F_2'(\xi_2)\right|\delta \\ &\leq \frac{2\pi}{t}\left|F_2'(\xi_2)\right|, \end{aligned} \tag{76}$$

where $0 < \xi_2 < \delta$ and by lemma 4 we have $|F_2'(\xi_2)| \leq \mathcal{F}\max\left\{H,W\right\}hG_0$. Then we can easily achieve Eq. (75).

Thirdly, we now prove the following inequality:

$$\left| \mathrm{g}\left[\tilde{f}_{\theta_k b}^{-1}\right](\hat{I}) - \tilde{f}_{\theta_k b}^{-1}\left[\mathrm{g}\right](\hat{I})\right| \leq 2\mathcal{F}\sum_{i=1}^{N}\left(\sum_{m=1}^{i}\frac{H_m F_0}{F_m} + 2\sum_{l=1}^{i}\frac{G_l}{F_l}\sum_{m=1}^{l-1}\frac{G_m F_0}{F_m} + 2\sum_{m=1}^{i}\frac{G_m G_0}{F_m} + H_0\right)h^2. \tag{77}$$

$\mathrm{g}(\cdot)$, an N-layer rotation equivariant CNN network, usually includes 1 input layer, $N-2$ intermediate layers, and 1 output layer. We can formally define it as :

$$\mathrm{g}(\cdot) = \hat{\Upsilon}\left[\hat{\Phi}_{N-1}\cdots\hat{\Phi}_{i+1}\left[\hat{\Phi}_i\cdots\hat{\Phi}_2\left[\hat{\Psi}\right]\cdots\right]\right](\cdot). \tag{78}$$

Then we have

$$\begin{aligned}
&\left| \mathrm{g}\left[\tilde{f}_{\theta_k b}^{-1}\right](\hat{I}) - \tilde{f}_{\theta_k b}^{-1}\left[\mathrm{g}\right](\hat{I})\right| \\
=&\left|\hat{\Upsilon}\left[\hat{\Phi}_{N-1}\cdots\hat{\Phi}_{i+1}\left[\hat{\Phi}_i\cdots\hat{\Phi}_2\left[\hat{\Psi}\left[\tilde{f}_{\theta_k b}^{-1}\right]\right]\cdots\right]\right](\hat{I}) - \tilde{f}_{\theta_k b}^{-1}\left[\hat{\Upsilon}\left[\hat{\Phi}_{N-1}\cdots\hat{\Phi}_{i+1}\left[\hat{\Phi}_i\cdots\hat{\Phi}_2\left[\hat{\Psi}\right]\cdots\right]\right]\right](\hat{I})\right| \\
\leq&\left|\hat{\Upsilon}\left[\hat{\Phi}_{N-1}\cdots\hat{\Phi}_{i+1}\left[\hat{\Phi}_i\cdots\hat{\Phi}_2\left[\hat{\Psi}\left[\tilde{f}_{\theta_k b}^{-1}\right]\right]\cdots\right]\right](\hat{I}) - \hat{\Upsilon}\left[\hat{\Phi}_{N-1}\cdots\hat{\Phi}_{i+1}\left[\hat{\Phi}_i\cdots\hat{\Phi}_2\left[\tilde{f}_{\theta_k b}^{-1}\left[\hat{\Psi}\right]\right]\cdots\right]\right](\hat{I})\right| \\
&+\left|\hat{\Upsilon}\left[\hat{\Phi}_{N-1}\cdots\hat{\Phi}_{i+1}\left[\hat{\Phi}_i\cdots\hat{\Phi}_2\left[\tilde{f}_{\theta_k b}^{-1}\left[\hat{\Psi}\right]\right]\cdots\right]\right](\hat{I}) - \hat{\Upsilon}\left[\hat{\Phi}_{N-1}\cdots\hat{\Phi}_{i+1}\left[\hat{\Phi}_i\cdots\tilde{f}_{\theta_k b}^{-1}\left[\hat{\Phi}_2\left[\hat{\Psi}\right]\right]\cdots\right]\right](\hat{I})\right| \\
&\cdots \\
&+\left|\hat{\Upsilon}\left[\hat{\Phi}_{N-1}\left[\tilde{f}_{\theta_k b}^{-1}\cdots\hat{\Phi}_{i+1}\left[\hat{\Phi}_i\cdots\hat{\Phi}_2\left[\hat{\Psi}\right]\cdots\right]\right]\right](\hat{I}) - \hat{\Upsilon}\left[\tilde{f}_{\theta_k b}^{-1}\left[\hat{\Phi}_{N-1}\cdots\hat{\Phi}_{i+1}\left[\hat{\Phi}_i\cdots\hat{\Phi}_2\left[\hat{\Psi}\right]\right]\cdots\right]\right](\hat{I})\right| \\
&+\left|\hat{\Upsilon}\left[\tilde{f}_{\theta_k b}^{-1}\left[\hat{\Phi}_{N-1}\cdots\hat{\Phi}_{i+1}\left[\hat{\Phi}_i\cdots\hat{\Phi}_2\left[\hat{\Psi}\right]\right]\cdots\right]\right](\hat{I}) - \tilde{f}_{\theta_k b}^{-1}\left[\hat{\Upsilon}\left[\hat{\Phi}_{N-1}\cdots\hat{\Phi}_{i+1}\left[\hat{\Phi}_i\cdots\hat{\Phi}_2\left[\hat{\Psi}\right]\right]\cdots\right]\right](\hat{I})\right|.
\end{aligned} \tag{79}$$

We denote δ_1, δ_i $(i=2,3,\cdots,N-1)$, and δ_N as the filter indexes of the input layer, i^{th} intermediate layer and output layer, respectively. The input channel number of the i^{th} layer is set as $c_{i-1}=n_{i-1}$.

1) For the input layer, with Eqs. (52), (55) and (58), let x denote the coordinate of position (k,l), then we have

$$
\begin{aligned}
&\left|\left(\hat{\Upsilon}\left[\hat{\Phi}_{N-1}\cdots\hat{\Phi}_{i+1}\left[\hat{\Phi}_i\cdots\hat{\Phi}_2\left[\hat{\Psi}\left[\tilde{f}^{-1}_{\theta_k b}\right]\right]\cdots\right]\right](\hat{I})-\hat{\Upsilon}\left[\hat{\Phi}_{N-1}\cdots\hat{\Phi}_{i+1}\left[\hat{\Phi}_i\cdots\hat{\Phi}_2\left[\tilde{f}^{-1}_{\theta_k b}\left[\hat{\Psi}\right]\right]\cdots\right]\right](\hat{I})\right)^{c_N}_{ij}\right| \\
=&\left|\sum_{\substack{c_{N-1}\\ B_{N-1}\in S\\ \delta_N\in\Lambda}}\cdots\sum_{\substack{c_1\\ A\in S\\ \delta_2\in\Lambda}}\sum_{\substack{c_0\\ \delta_1\in\Lambda}}\varphi^N_{c_{N-1}c_N}(B^{-1}_{N-1}\delta_N)\cdots\varphi^1_{c_0c_1}\left(A^{-1}\delta_1\right)r_{c_0}\left(A_{\theta_k}(x-\delta_N-\cdots-\delta_2-\delta_1+b)\right)\right. \\
&\left.-\sum_{\substack{c_{N-1}\\ B_{N-1}\in S\\ \delta_N\in\Lambda}}\cdots\sum_{\substack{c_1\\ A\in S\\ \delta_2\in\Lambda}}\sum_{\substack{c_0\\ \delta_1\in\Lambda}}\varphi^N_{c_{N-1}c_N}(B^{-1}_{N-1}\delta_N)\cdots\varphi^1_{c_0c_1}\left(A^{-1}A^{-1}_{\theta_k}\delta_1\right)r_{c_0}\left(A_{\theta_k}(x-\delta_N-\cdots-\delta_2+b)-\delta_1\right)\right| \\
=&\left|\sum_{\substack{c_{N-1}\\ B_{N-1}\in S\\ \delta_N\in\Lambda}}\cdots\sum_{\substack{c_1\\ A\in S\\ \delta_2\in\Lambda}}\varphi^N_{c_{N-1}c_N}(B^{-1}_{N-1}\delta_N)\cdots\varphi^2_{Ac_1c_2}(B^{-1}_2\delta_2)\right. \\
&\left.\left(\sum_{\substack{c_0\\ \delta_1\in\Lambda}}\varphi^1_{c_0c_1}\left(A^{-1}\delta_1\right)r\left(A_{\theta_k}(x-\delta_N-\cdots\delta_1+b)\right)-\sum_{\substack{c_0\\ \delta_1\in\Lambda}}\varphi^1_{c_0c_1}\left(A^{-1}A^{-1}_{\theta_k}\delta_1\right)r_{c_0}\left(A_{\theta_k}(x-\delta_N-\cdots\delta_2+b)-\delta_1\right)\right)\right| \\
\leq&\sum_{\substack{c_{N-1}\\ B_{N-1}\in S\\ \delta_N\in\Lambda}}\cdots\sum_{\substack{c_1\\ A\in S\\ \delta_2\in\Lambda}}\left|\varphi^N_{c_{N-1}c_N}(B^{-1}_{N-1}\delta_N)\right|\cdots\left|\varphi^2_{Ac_1c_2}(B^{-1}_2\delta_2)\right| \\
&\left|\sum_{\substack{c_0\\ \delta_1\in\Lambda}}\varphi^1_{c_0c_1}\left(A^{-1}\delta_1\right)r\left(A_{\theta_k}(x-\delta_N-\cdots-\delta_1+b)\right)-\sum_{\substack{c_0\\ \delta_1\in\Lambda}}\varphi^1_{c_0c_1}\left(A^{-1}A^{-1}_{\theta_k}\delta_1\right)r_{c_0}\left(A_{\theta_k}(x-\delta_N-\cdots-\delta_2+b)-\delta_1\right)\right| \\
\leq&\sum_{\substack{c_{N-1}\\ B_{N-1}\in S\\ \delta_N\in\Lambda}}\cdots\sum_{\substack{c_1\\ A\in S\\ \delta_2\in\Lambda}}\sum_{c_0}F_N\cdots F_2\left|\sum_{\delta_1\in\Lambda}\varphi^1_{c_0c_1}\left(A^{-1}\delta_1\right)r\left(A_{\theta_k}(x-\delta_N\cdots-\delta_1+b)\right)\right. \\
&\left.-\sum_{\delta_1\in\Lambda}\varphi^1_{c_0c_1}\left(A^{-1}A^{-1}_{\theta_k}\delta_1\right)r_{c_0}\left(A_{\theta_k}(x-\delta_N-\cdots-\delta_2+b)-\delta_1\right)\right|.
\end{aligned}
\tag{80}
$$

Let us denote $\hat{x} = x - \delta_N - \delta_{N-1} - \cdots - \delta_2 + b$. Utilizing Eq. (35) from Remark 2 for the input layer, we can deduce the following result:

$$
\begin{aligned}
&\left| \sum_{\delta_1 \in \Lambda} \varphi^1_{c_0 c_1}\left(A^{-1}\delta_1\right) r\left(A_{\theta_k}(x - \delta_N \cdots - \delta_1 + b)\right) \right. \\
&\qquad\qquad \left. - \sum_{\delta_1 \in \Lambda} \varphi^1_{c_0 c_1}\left(A^{-1} A^{-1}_{\theta_k}\delta_1\right) r_{c_0}\left(A_{\theta_k}(x - \delta_N - \cdots - \delta_2 + b) - \delta_1\right) \right| \\
= &\left| \sum_{\delta_1 \in \Lambda} \varphi^1_{c_0 c_1}\left(A^{-1}\delta_1\right) r\left(A_{\theta_k}(\hat{x} - \delta_1)\right) \right. \\
&\qquad\qquad \left. - \sum_{\delta_1 \in \Lambda} \varphi^1_{c_0 c_1}\left(A^{-1} A^{-1}_{\theta_k}\delta_1\right) r_{c_0}\left(A_{\theta_k}\hat{x} - \delta_1\right) \right| \\
\leq & n_0 \frac{C_1}{2}(p+1)^2 h^2,
\end{aligned}
\tag{81}
$$

where we do not specifically indicate the numbers of input and output channels, i.e. $\varphi^1(x) = \varphi^1_{c_0 c_1}(x)$, and we have $C_1 = H_1 F_0 + F_1 H_0 + 2G_1 G_0$.
Therefore, according to Eqs. (80) and (81), we have

$$
\begin{aligned}
&\left| \left(\hat{\Upsilon}\left[\hat{\Phi}_{N-1} \cdots \hat{\Phi}_{i+1}\left[\hat{\Phi}_i \cdots \hat{\Phi}_2\left[\hat{\Psi}\left[\tilde{f}^{-1}_{\theta_k b}\right]\right] \cdots\right]\right](\hat{I}) \right. \right. \\
&\qquad\qquad \left. \left. - \hat{\Upsilon}\left[\hat{\Phi}_{N-1} \cdots \hat{\Phi}_{i+1}\left[\hat{\Phi}_i \cdots \hat{\Phi}_2\left[\tilde{f}^{-1}_{\theta_k b}\left[\hat{\Psi}\right]\right] \cdots\right]\right](\hat{I}) \right)^{c_N}_{ij} \right| \\
\leq & n_{N-1} p^2 F_N n_{N-2} p^2 F_{N-1} \cdots n_1 p^2 F_2 n_0 \frac{C_1}{2}(p+1)^2 h^2 \\
\leq & \left(\prod_{k=2}^{N} n_{k-1} p^2 F_k \right) n_0 \frac{(p+1)^2 h^2}{2}\left(H_1 F_0 + F_1 H_0 + 2G_1 G_0\right) \\
\leq & 2\mathcal{F}\left(\frac{H_1}{F_1} F_0 + H_0 + 2\frac{G_1}{F_1} G_0 \right) h^2.
\end{aligned}
\tag{82}
$$

2) For the any i^{th} intermediate layer, $1 < i < N$. We have:

$$
\begin{aligned}
&\left| \left(\hat{\Upsilon}\left[\hat{\Phi}_{N-1} \cdots \hat{\Phi}_i\left[\tilde{f}^{-1}_{\theta_k b}\left[\hat{\Phi}_{i-1} \cdots \hat{\Phi}_2\left[\hat{\Psi}\right] \cdots\right]\right]\right](\hat{I}) \right. \right. \\
&\qquad\qquad \left. \left. - \hat{\Upsilon}\left[\hat{\Phi}_{N-1} \cdots \hat{\Phi}_{i+1}\left[\tilde{f}^{-1}_{\theta_k b}\left[\hat{\Phi}_i \cdots \hat{\Phi}_2\left[\hat{\Psi}\right] \cdots\right]\right]\right](\hat{I}) \right)^{c_N}_{ij} \right| \\
= &\left| \sum_{\substack{c_{N-1} \\ B_{N-1} \in S \\ \delta_N \in \Lambda}} \cdots \sum_{\substack{c_{i-1} \\ B_{i-1} \in S \\ \delta_i \in \Lambda}} \varphi^N_{c_{N-1} c_N}(B^{-1}_{N-1}\delta_N) \cdots \varphi^i_{B_{i-1} c_{i-1} c_i}(B^{-1}_i \delta_i) \right. \\
&\qquad\qquad e^{i-1}_{c_{i-1}}\left(A_{\theta_k}(x - \delta_N - \cdots - \delta_i + b), A_{\theta_k} B_{i-1}\right) \\
&- \sum_{\substack{c_{N-1} \\ B_{N-1} \in S \\ \delta_N \in \Lambda}} \cdots \sum_{\substack{c_{i-1} \\ B_{i-1} \in S \\ \delta_i \in \Lambda}} \varphi^N_{c_{N-1} c_N}(B^{-1}_{N-1}\delta_N) \cdots \varphi^i_{B_{i-1} c_{i-1} c_i}(B^{-1}_i A^{-1}_{\theta_k}\delta_i) \\
&\qquad\qquad \left. e^{i-1}_{c_{i-1}}\left(A_{\theta_k}(x - \delta_N - \cdots - \delta_{i+1} + b) - \delta_i, B_{i-1}\right) \right|
\end{aligned}
\tag{83}
$$

$$
\begin{aligned}
&\leq \Bigg| \sum_{\substack{c_{N-1}\\ B_{N-1}\in S\\ \delta_N\in\Lambda}} \cdots \sum_{\substack{c_i\\ B_i\in S\\ \delta_{i+1}\in\Lambda}} \varphi^N_{c_{N-1}c_N}(B^{-1}_{N-1}\delta_N)\varphi^{N-1}_{B_{N-2}c_{N-2}c_{N-1}}(B^{-1}_{N-1}\delta_{N-1})\cdots\varphi^{i+1}_{B_ic_ic_{i+1}}(B^{-1}_{i+1}\delta_{i+1}) \\
&\quad\Bigg(\sum_{\substack{c_{i-1}\\ B_{i-1}\in S\\ \delta_i\in\Lambda}} \varphi^i_{B_{i-1}c_{i-1}c_i}(B^{-1}_i\delta_i)e^{i-1}_{c_{i-1}}(A_{\theta_k}(x-\delta_N-\cdots-\delta_{i+1}-\delta_i+b), A_{\theta_k}B_{i-1}) \\
&\quad - \sum_{\substack{c_{i-1}\\ B_{i-1}\in S\\ \delta_i\in\Lambda}} \varphi^i_{B_{i-1}c_{i-1}c_i}(B^{-1}_iA^{-1}_{\theta_k}\delta_i)e^{i-1}_{c_{i-1}}(A_{\theta_k}(x-\delta_N-\cdots-\delta_{i+1}+b)-\delta_i, B_{i-1})\Bigg)\Bigg| \\
&\leq \sum_{\substack{c_{N-1}\\ B_{N-1}\in S\\ \delta_N\in\Lambda}} \sum_{\substack{c_{N-2}\\ B_{N-2}\in S\\ \delta_{N-1}\in\Lambda}} \cdots \sum_{\substack{c_i\\ B_i\in S\\ \delta_{i+1}\in\Lambda}} F_NF_{N-1}\cdots F_{i+1} \\
&\quad\Bigg|\Bigg(\sum_{\substack{c_{i-1}\\ B_{i-1}\in S\\ \delta_i\in\Lambda}} \varphi^i_{B_{i-1}c_{i-1}c_i}(B^{-1}_i\delta_i)e^{i-1}_{c_{i-1}}(A_{\theta_k}(x-\delta_N-\cdots-\delta_{i+1}-\delta_i+b), A_{\theta_k}B_{i-1}) \\
&\quad - \sum_{\substack{c_{i-1}\\ B_{i-1}\in S\\ \delta_i\in\Lambda}} \varphi^i_{B_{i-1}c_{i-1}c_i}(B^{-1}_iA^{-1}_{\theta_k}\delta_i)e^{i-1}_{c_{i-1}}(A_{\theta_k}(x-\delta_N-\cdots-\delta_{i+1}+b)-\delta_i, B_{i-1})\Bigg)\Bigg|.
\end{aligned}
$$

Let us denote $\hat{x} = x - \delta_N - \cdots - \delta_{i+1} + b$. Then, by Eq. (35) in Remark 2, we have:

$$
\begin{aligned}
&\Bigg| \sum_{\substack{c_{i-1}\\ B_{i-1}\in S\\ \delta_i\in\Lambda}} \varphi^i_{B_{i-1}c_{i-1}c_i}(B^{-1}_i\delta_i)e^{i-1}_{c_{i-1}}\,(A_{\theta_k}(\hat{x}-\delta_i), A_{\theta_k}B_{i-1}) \\
&\qquad\qquad - \sum_{\substack{c_{i-1}\\ B_{i-1}\in S\\ \delta_i\in\Lambda}} \varphi^i_{B_{i-1}c_{i-1}c_i}(B^{-1}_iA_{\theta_k^{-1}}\delta_i)e^{i-1}_{c_{i-1}}\,(A_{\theta_k}\hat{x}-\delta_i, B_{i-1})\Bigg| \\
&= \sum_{c_{i-1}} \Bigg| \sum_{\substack{B_{i-1}\in S\\ \delta_i\in\Lambda}} \varphi^i_{B_{i-1}c_{i-1}c_i}(B^{-1}_i\delta_i)e^{i-1}_{c_{i-1}}\,(A_{\theta_k}(\hat{x}-\delta_i), A_{\theta_k}B_{i-1}) \\
&\qquad\qquad - \sum_{\substack{B_{i-1}\in S\\ \delta_i\in\Lambda}} \varphi^i_{B_{i-1}c_{i-1}c_i}(B^{-1}_iA^{-1}_{\theta_k}\delta_i)e^{i-1}_{c_{i-1}}\,(A_{\theta_k}\hat{x}-\delta_i, B_{i-1})\Bigg| \\
&\leq n_{i-1}\frac{C_i}{2}(p+1)^2h^2,
\end{aligned}
\tag{84}
$$

where we do not specifically indicate the numbers of input and output channels, i.e. $\varphi^i(x) = \varphi^i_{Ac_{i-1}c_i}(x)$, and we have
$C_i = \sup\left(\left\|\nabla^2\varphi^i(x)\right\| \left|e^{i-1}_{c_{i-1}}(x,B)\right| + \left|\varphi^i(x)\right| \left\|\nabla^2 e^{i-1}_{c_{i-1}}(x,B)\right\| + 2\left\|\nabla\varphi^i(x)\right\| \left\|\nabla e^{i-1}_{c_{i-1}}(x,B)\right\|\right)$.
Therefore, according to Eqs. (83) and (84), we have

$$\begin{aligned}
&\Bigg|\Bigg(\hat{\Upsilon}\left[\hat{\Phi}_{N-1}\cdots\hat{\Phi}_i\left[\tilde{f}^{-1}_{\theta_k b}\left[\hat{\Phi}_{i-1}\cdots\hat{\Phi}_2\left[\hat{\Psi}\right]\cdots\right]\right]\right](\hat{I}) \\
&\qquad\qquad - \hat{\Upsilon}\left[\hat{\Phi}_{N-1}\cdots\hat{\Phi}_{i+1}\left[\tilde{f}^{-1}_{\theta_k b}\left[\hat{\Phi}_i\cdots\hat{\Phi}_2\left[\hat{\Psi}\right]\cdots\right]\right]\right](\hat{I})\Bigg)^{c_N}_{ij}\Bigg| \\
\leq& n_{N-1}p^2F_N\cdots n_ip^2F_{i+1}n_{i-1}\frac{C_i}{2}(p+1)^2h^2 \\
=& \left(\prod_{k=i+1}^{N} n_{k-1}p^2F_k\right) n_{i-1}\frac{C_i}{2}(p+1)^2h^2.
\end{aligned} \tag{85}$$

Substituting Eqs. (63), (64) and (65) into Eq. (85), denoting $\mathcal{F}_{i-1} = \prod_{k=1}^{i-1} n_{k-1}p^2F_k$, then we have

$$\begin{aligned}
&\left|\left(\hat{\Upsilon}\left[\hat{\Phi}_{N-1}\cdots\hat{\Phi}_i\left[\tilde{f}^{-1}_{\theta_k b}\left[\hat{\Phi}_{i-1}\cdots\hat{\Phi}_2\left[\hat{\Psi}\right]\cdots\right]\right]\right](\hat{I}) - \hat{\Upsilon}\left[\hat{\Phi}_{N-1}\cdots\hat{\Phi}_{i+1}\left[\tilde{f}^{-1}_{\theta_k b}\left[\hat{\Phi}_i\cdots\hat{\Phi}_2\left[\hat{\Psi}\right]\cdots\right]\right]\right](\hat{I})\right)^{c_N}_{ij}\right| \\
\leq& \left(\prod_{k=i+1}^{N} n_{k-1}p^2F_k\right)\frac{n_{i-1}(p+1)^2h^2}{2} \\
&\left(\left\|\nabla^2\varphi^i(x)\right\| \left|e^{i-1}_{c_{i-1}}(x,B)\right| + \left|\varphi^i(x)\right| \left\|\nabla^2 e^{i-1}_{c_{i-1}}(x,B)\right\| + 2\left\|\nabla\varphi^i(x)\right\| \left\|\nabla e^{i-1}_{c_{i-1}}(x,B)\right\|\right) \\
\leq& 2\left(\prod_{k=i}^{N} n_{k-1}p^2F_k\right)\left(\frac{H_i}{F_i}\left|e^{i-1}_{c_{i-1}}(x,B)\right| + \left\|\nabla^2 e^{i-1}_{c_{i-1}}(x,B)\right\| + 2\frac{G_i}{F_i}\left\|\nabla e^{i-1}_{c_{i-1}}(x,B)\right\|\right)h^2 \\
\leq& 2\left(\prod_{k=i}^{N} n_{k-1}p^2F_k\right)\mathcal{F}_{i-1} \\
&\left(\frac{H_iF_0}{F_i} + \sum_{m=1}^{i-1}\frac{H_mF_0}{F_m} + 2\sum_{l=1}^{i-1}\frac{G_l}{F_l}\sum_{m=1}^{l-1}\frac{G_mF_0}{F_m} + 2\sum_{m=1}^{i-1}\frac{G_mG_0}{F_m} + H_0 + \sum_{m=1}^{i-1}2\frac{G_iG_mF_0}{F_iF_m} + 2\frac{G_iG_0}{F_i}\right)h^2 \\
\leq& 2\mathcal{F}\left(\sum_{m=1}^{i}\frac{H_mF_0}{F_m} + 2\sum_{l=1}^{i}\frac{G_l}{F_l}\sum_{m=1}^{l-1}\frac{G_mF_0}{F_m} + 2\sum_{m=1}^{i}\frac{G_mG_0}{F_m} + H_0\right)h^2.
\end{aligned} \tag{86}$$

3) For the output layer, with Eqs. (52), (55) and (58) we have

$$\begin{aligned}
&\left|\left(\hat{\Upsilon}\left[\tilde{f}^{-1}_{\theta_k b}\left[\hat{\Phi}_{N-1}\cdots\hat{\Phi}_{i+1}\left[\hat{\Phi}_i\cdots\hat{\Phi}_2\left[\hat{\Psi}\right]\cdots\right]\right]\right](\hat{I}) - \tilde{f}^{-1}_{\theta_k b}\left[\hat{\Upsilon}\left[\hat{\Phi}_{N-1}\cdots\hat{\Phi}_{i+1}\left[\hat{\Phi}_i\cdots\hat{\Phi}_2\left[\hat{\Psi}\right]\cdots\right]\right]\right](\hat{I})\right)^{c_N}_{ij}\right| \\
=& \Bigg|\sum_{\substack{c_{N-1}\\ B_{N-1}\in S\\ \delta_N\in\Lambda}} \varphi^N_{c_{N-1}c_N}(B^{-1}_{N-1}\delta_N)e^{N-1}_{c_{N-1}}\left(A_{\theta_k}(x-\delta_N+b), A_{\theta_k}B_{N-1}\right) \\
&\qquad - \sum_{\substack{c_{N-1}\\ B_{N-1}\in S\\ \delta_N\in\Lambda}} \varphi^N_{c_{N-1}c_N}(B^{-1}_{N-1}A^{-1}_{\theta_k}\delta_N)e^{N-1}_{c_{N-1}}\left(A_{\theta_k}(x+b)-\delta_N, B_{N-1}\right)\Bigg|.
\end{aligned}$$

Then, by Eq. (35) from Remark 2 for the output, we have:

$$\begin{aligned}&\left|\left(\hat{\Upsilon}\left[\tilde{f}^{-1}_{\theta_k b}\left[\hat{\Phi}_{N-1}\cdots\hat{\Phi}_{i+1}\left[\hat{\Phi}_i\cdots\hat{\Phi}_2\left[\hat{\Psi}\right]\cdots\right]\right]\right](\hat{I}) - \tilde{f}^{-1}_{\theta_k b}\left[\hat{\Upsilon}\left[\hat{\Phi}_{N-1}\cdots\hat{\Phi}_{i+1}\left[\hat{\Phi}_i\cdots\hat{\Phi}_2\left[\hat{\Psi}\right]\cdots\right]\right]\right](\hat{I})\right)^{c_N}_{ij}\right| \\
\le & \sum_{c_{N-1}}\left|\sum_{\substack{B_{N-1}\in S\\ \delta_N\in\Lambda}}\varphi^N_{c_{N-1}c_N}(B^{-1}_{N-1}\delta_N)e^{N-1}_{c_{N-1}}\left(DA_{\theta_k}\left(x-\delta_N+b\right), A_{\theta_k}B_{N-1}\right)\right. \\
&\left. - \sum_{\substack{B_{N-1}\in S\\ \delta_N\in\Lambda}}\varphi^N_{c_{N-1}c_N}(B^{-1}_{N-1}A^{-1}_{\theta_k}\delta_N)e^{N-1}_{c_{N-1}}\left(A_{\theta_k}(x+b)-\delta_N, B_{N-1}\right)\right| \\
\le & n_{N-1}\frac{C_N}{2}(p+1)^2h^2,
\end{aligned} \tag{87}$$

where we do not specifically indicate the numbers of input and output channels, i.e. $\varphi^N(x) = \varphi^N_{c_{N-1}c_N}(x)$, and we have
$C_N = \sup\left(\left\|\nabla^2\varphi^N(x)\right\|\left|e^{N-1}_{c_{N-1}}(x,B)\right| + \left|\varphi^N(x)\right|\left\|\nabla^2 e^{N-1}_{c_{N-1}}(x,B)\right\| + 2\left\|\nabla\varphi^N(x)\right\|\left\|\nabla e^{N-1}_{c_{N-1}}(x,B)\right\|\right)$.

Substituting Eqs. (63), (64) and (65) into Eq. (87), denoting $\mathcal{F}_{N-1} = \prod_{k=1}^{N-1} n_{k-1}p^2F_k$, then we have

$$\begin{aligned}&\left|\left(\hat{\Upsilon}\left[\tilde{f}^{-1}_{\theta_k b}\left[\hat{\Phi}_{N-1}\cdots\hat{\Phi}_{i+1}\left[\hat{\Phi}_i\cdots\hat{\Phi}_2\left[\hat{\Psi}\right]\cdots\right]\right]\right](\hat{I}) - \tilde{f}^{-1}_{\theta_k b}\left[\hat{\Upsilon}\left[\hat{\Phi}_{N-1}\cdots\hat{\Phi}_{i+1}\left[\hat{\Phi}_i\cdots\hat{\Phi}_2\left[\hat{\Psi}\right]\cdots\right]\right]\right](\hat{I})\right)^{c_N}_{ij}\right| \\
\le & \frac{n_{N-1}(p+1)^2h^2}{2}\left(\left\|\nabla^2\varphi^N(x)\right\|\left|e^{N-1}_{c_{N-1}}(x,B)\right| + \left|\varphi^N(x)\right|\left\|\nabla^2 e^{N-1}_{c_{N-1}}(x,B)\right\| + 2\left\|\nabla\varphi^N(x)\right\|\left\|\nabla e^{N-1}_{c_{N-1}}(x,B)\right\|\right) \\
\le & 2n_{N-1}p^2F_N\left(\frac{H_N}{F_N}\left|e^{N-1}_{c_{N-1}}(x,B)\right| + \left\|\nabla^2 e^{N-1}_{c_{N-1}}(x,B)\right\| + 2\frac{G_N}{F_N}\left\|\nabla e^{N-1}_{c_{N-1}}(x,B)\right\|\right)h^2 \\
\le & 2n_{N-1}p^2F_N\mathcal{F}_{N-1} \\
&\left(\frac{H_N}{F_N}F_0 + \sum_{m=1}^{N-1}\frac{H_mF_0}{F_m} + 2\sum_{l=1}^{N-1}\frac{G_l}{F_l}\sum_{m=1}^{l-1}\frac{G_mF_0}{F_m} + 2\sum_{m=1}^{N-1}\frac{G_mG_0}{F_m} + H_0 + \sum_{m=1}^{N-1}2\frac{G_NG_mF_0}{F_NF_m} + 2\frac{G_NG_0}{F_N}\right)h^2 \\
\le & 2\mathcal{F}\left(\sum_{m=1}^{N}\frac{H_mF_0}{F_m} + 2\sum_{l=1}^{N}\frac{G_l}{F_l}\sum_{m=1}^{l-1}\frac{G_mF_0}{F_m} + 2\sum_{m=1}^{N}\frac{G_mG_0}{F_m} + H_0\right)h^2.
\end{aligned} \tag{88}$$

4) Substituting Eqs. (82), (86) and (88) into Eq. (79) we can get:

$$
\begin{aligned}
&\left|\mathrm{g}\left[\tilde{f}_{\theta_k b}^{-1}\right](\hat{I})-\tilde{f}_{\theta_k b}^{-1}[\mathrm{g}](\hat{I})\right| \\
\leq & 2\mathcal{F}\left(\frac{H_1}{F_1}F_0+H_0+2\frac{G_1}{F_1}G_0\right)h^2 \\
&+\sum_{i=2}^{N-1}2\mathcal{F}\left(\sum_{m=1}^{i}\frac{H_mF_0}{F_m}+2\sum_{l=1}^{i}\frac{G_l}{F_l}\sum_{m=1}^{l-1}\frac{G_mF_0}{F_m}+2\sum_{m=1}^{i}\frac{G_mG_0}{F_m}+H_0\right)h^2 \\
&+2\mathcal{F}\left(\sum_{m=1}^{N}\frac{H_mF_0}{F_m}+2\sum_{l=1}^{N}\frac{G_l}{F_l}\sum_{m=1}^{l-1}\frac{G_mF_0}{F_m}+2\sum_{m=1}^{N}\frac{G_mG_0}{F_m}+H_0\right)h^2 \\
\leq & 2\mathcal{F}\sum_{i=1}^{N}\left(\sum_{m=1}^{i}\frac{H_mF_0}{F_m}+2\sum_{l=1}^{i}\frac{G_l}{F_l}\sum_{m=1}^{l-1}\frac{G_mF_0}{F_m}+2\sum_{m=1}^{i}\frac{G_mG_0}{F_m}+H_0\right)h^2.
\end{aligned}
\tag{89}
$$

Therefore, we achieve Eq. (77).

Finally, we will provide the error analysis for the N-layer rotation equivariant CNN network. Substituting Eqs. (73), (75) and (77) into Eq. (72), we can get:

$$
\begin{aligned}
&\left|\tilde{f}_{\theta b}^{-1}\,\mathrm{g}\left[\tilde{f}_{\theta b}\right](I)-[\mathrm{g}](I)\right| \\
\leq & \frac{2\pi}{t}\mathcal{F}\left(\max\{H,W\}+N(p+1)\right)hG_0+\frac{2\pi}{t}\mathcal{F}\max\{H,W\}hG_0 \\
&+2\mathcal{F}\sum_{i=1}^{N}\left(\sum_{m=1}^{i}\frac{H_mF_0}{F_m}+2\sum_{l=1}^{i}\frac{G_l}{F_l}\sum_{m=1}^{l-1}\frac{G_mF_0}{F_m}+2\sum_{m=1}^{i}\frac{G_mG_0}{F_m}+H_0\right)h^2 \\
\leq & \frac{2\pi}{t}\mathcal{F}\left(2\max\{H,W\}+N(p+1)\right)hG_0 \\
&+2\mathcal{F}\sum_{i=1}^{N}\left(\sum_{m=1}^{i}\frac{H_mF_0}{F_m}+2\sum_{l=1}^{i}\frac{G_l}{F_l}\sum_{m=1}^{l-1}\frac{G_mF_0}{F_m}+2\sum_{m=1}^{i}\frac{G_mG_0}{F_m}+H_0\right)h^2
\end{aligned}
\tag{90}
$$

Next, in order to get a more concise form, we further scale the entire error bound. By Eq. (90), we have:

$$
\begin{aligned}
&\left|\tilde{f}_{\theta b}^{-1}\,\mathrm{g}\left[\tilde{f}_{\theta b}\right](I)-[\mathrm{g}](I)\right| \\
= & \frac{2\pi}{t}\mathcal{F}\left(2\max\{H,W\}p^{-1}+N(p+1)p^{-1}\right)phG_0 \\
&+2\mathcal{F}\sum_{i=1}^{N}(N+1-i)\left(\frac{H_iF_0}{F_i}+2\frac{G_i}{F_i}\sum_{m=1}^{i-1}\frac{G_mF_0}{F_m}+2\frac{G_iG_0}{F_i}\right)h^2+2\mathcal{F}NH_0h^2 \\
\leq & \frac{2\pi}{t}\mathcal{F}\left(2\max\{H,W\}p^{-1}+2N\right)phG_0 \\
&+2\mathcal{F}N\sum_{i=1}^{N}\left(\frac{H_iF_0}{F_i}+2\frac{G_i}{F_i}\sum_{m=1}^{i-1}\frac{G_mF_0}{F_m}+2\frac{G_iG_0}{F_i}\right)h^2+2\mathcal{F}NH_0h^2 \\
\leq & 2N\mathcal{F}\sum_{i=1}^{N}\left(\frac{H_iF_0}{F_i}+2\frac{G_i}{F_i}\sum_{m=1}^{i-1}\frac{G_mF_0}{F_m}+2\frac{G_iG_0}{F_i}+H_0\right)h^2 \\
&+2\pi G_0\mathcal{F}\left(2\max\{H,W\}p^{-1}+2N\right)pht^{-1}
\end{aligned}
\tag{91}
$$

If we denote

$$
\begin{aligned}
&C_1=2N\mathcal{F}\cdot\sum_{i=1}^{N}\left(\frac{H_iF_0}{F_i}+2\frac{G_i}{F_i}\sum_{m=1}^{i-1}\frac{G_mF_0}{F_m}+2\frac{G_iG_0}{F_i}+H_0\right), \\
&C_2=2\pi G_0\mathcal{F}\left(2\max\{H,W\}p^{-1}+2N\right).
\end{aligned}
\tag{92}
$$

Then we can obtain the error bound of the N-layer rotation equivariant CNN network as Eq. (70)

□

Lemma 5. *Based on the same conditions, for an arbitrary $0 \le \theta \le 2\pi$, $A_\theta \in S$ denotes the rotation matrix, $b \in \mathbb{R}^2$ denotes the translation, the following result is satisfied:*

$$\left\| \mathrm{g}\left[\tilde{f}_{\theta b}\right](I) - \tilde{f}_{\theta b}\left[\mathrm{g}\right](I) \right\|_\infty \le C_1 h^2 + C_2 pht^{-1}, \tag{93}$$

where C_1 and C_2 are defined in (92).

The proof of Lemma 5 is similar to Theorem 1 of [38]. Please refer to [38] for more details.

A.4 Proposition 1 and the Proof

Based on Theorem 1, we proceed to present the Proposition 1 in the main text and its proof.

Proposition 1. *For images I_0 and I_j with size $H \times W \times n_0$, and a N-layer rotation-translation equivariant CNN network $\mathrm{g}(\cdot)$, whose channel number of the i^{th} layer is n_i, rotation equivariant subgroup is $S \leqslant O(2)$, $|S| = t$, and activation function is set as ReLU. If the latent continuous function of the c^{th} channel of I_j and I_0 are denoted as $r_c : \mathbb{R}^2 \to \mathbb{R}$ and $\tilde{r_c} : \mathbb{R}^2 \to \mathbb{R}$, respectively, and the latent continuous function of any convolution filters in the i^{th} layer is denoted as $\varphi^i : \mathbb{R}^2 \to \mathbb{R}$, where $i \in \{1, \cdots, N\}$, $c \in \{1, \cdots, n_0\}$, for any $x \in \mathbb{R}^2$, the following conditions are satisfied:*

$$\begin{aligned} &|r_c(x)|, |\tilde{r}_c(x)| \le F_0, \|\nabla r_c(x)\|, \|\nabla \tilde{r}_c(x)\| \le G_0, \|\nabla^2 r_c(x)\|, \|\nabla^2 \tilde{r}_c(x)\| \le H_0, \\ &|\varphi^i(x)| \le F_i, \|\nabla \varphi^i(x)\| \le G_i, \|\nabla^2 \varphi^i(x)\| \le H_i, \\ &\forall \|x\| \ge {}^{(p+1)h}/2, \ \varphi_i(x) = 0, \end{aligned} \tag{94}$$

where p is the filter size, h is the mesh size, ∇ and ∇^2 denote the operators of gradient and Hessian matrix, respectively. For an arbitrary $0 \le \theta \le 2\pi$ and a feature map of equivariant convolution $Z = \mathrm{g}(I)$ with size $H \times W \times tC$, $A_\theta \in S$ denotes the rotation matrix, $b \in \mathbb{R}^2$ denotes the translation, the following result is satisfied:

$$\left\| \tilde{f}_{\theta b}^{-1}(Z_j) - Z_0 \right\|_\infty \le C_3 \left\| \tilde{f}_{\theta b}^{-1}(I_j) - I_0 \right\|_2 + C_1 h^2 + C_2 pht^{-1}, \tag{95}$$

where $\tilde{f}_{\theta b}$ is defined in Eq. (60) and

$$\begin{aligned} C_1 &= 2N\mathcal{F} \cdot \sum_{i=1}^{N} \left(\frac{H_i F_0}{F_i} + 2\frac{G_i}{F_i} \sum_{m=1}^{i-1} \frac{G_m F_0}{F_m} + 2\frac{G_i G_0}{F_i} + H_0 \right), \\ C_2 &= 2\pi G_0 \mathcal{F} \left(2\max\{H,W\} p^{-1} + 2N \right), \\ C_3 &= \prod_{k=1}^{N} n_{k-1} p^2 F_k. \end{aligned} \tag{96}$$

Proof. We can deduce that

$$\begin{aligned} &\left\| \tilde{f}_{\theta b}^{-1}(Z_j) - Z_0 \right\|_\infty \\ = &\left\| \tilde{f}_{\theta b}^{-1}\left[\mathrm{g}\right](I_j) - \mathrm{g}\left[\tilde{f}_{\theta b}^{-1}\right](I_j) + \mathrm{g}\left[\tilde{f}_{\theta b}^{-1}\right](I_j) - \mathrm{g}(I_0) \right\|_\infty \\ \le &\underbrace{\left\| \tilde{f}_{\theta b}^{-1}\left[\mathrm{g}\right](I_j) - \mathrm{g}\left[\tilde{f}_{\theta b}^{-1}\right](I_j) \right\|_\infty}_{\langle 1 \rangle} + \underbrace{\left\| \mathrm{g}\left[\tilde{f}_{\theta b}^{-1}\right](I_j) - \mathrm{g}(I_0) \right\|_\infty}_{\langle 2 \rangle} \end{aligned} \tag{97}$$

For the part $\langle 1 \rangle$, by exploiting Lemma 5, we have

$$\left\| \tilde{f}_{\theta b}^{-1}\left[\mathrm{g}\right](I_j) - \mathrm{g}\left[\tilde{f}_{\theta b}^{-1}\right](I_j) \right\|_\infty \le C_1 h^2 + C_2 pht^{-1}, \tag{98}$$

where C_1 and C_2 are defined in (92). For the part $\langle 2 \rangle$, consistent with the mathematical notation defined in Section 1.3., x_{kl} denotes the coordinates of the point (k, l). Let $\hat{r_c}(x) = r_c(A_\theta x + b)$, then $\hat{r_c}(x)$ is the latent function of $\tilde{f}_{\theta b}^{-1}(I_j)$. Besides,

$$|\hat{r_c}(x)| \leq F_0, \|\nabla \hat{r_c}(x)\| \leq G_0, \|\nabla^2 \hat{r_c}(x)\| \leq H_0. \tag{99}$$

Then we can deduce that

$$\begin{aligned}
&\left|\left(\mathrm{g}\left[\tilde{f}_{\theta b}^{-1}\right](I_j) - \mathrm{g}(I_0)\right)_{kl}\right| \\
&= \sum_{\substack{c_{N-1} \\ B_{N-1} \in S \\ \delta_N \in \Lambda}} \cdots \sum_{\substack{c_1 \\ A \in S \\ \delta_2 \in \Lambda}} \sum_{\substack{c_0 \\ \delta_1 \in \Lambda}} \varphi_{c_{N-1} c_N}^N (B_{N-1}^{-1} \delta_N) \cdots \varphi_{c_0 c_1}^1 \left(A^{-1} \delta_1\right) \\
&\qquad\qquad \left(\hat{r_c}\left(x_{kl} - \delta_N - \cdots - \delta_1\right) - \tilde{r_c}\left(x_{kl} - \delta_N - \cdots - \delta_1\right)\right) \\
&= \sum_{\substack{c_{N-1} \\ B_{N-1} \in S \\ \delta_N \in \Lambda}} \cdots \sum_{\substack{c_1 \\ A \in S \\ \delta_2 \in \Lambda}} \sum_{\substack{c_0 \\ \delta_1 \in \Lambda}} \left|\varphi_{c_{N-1} c_N}^N (B_{N-1}^{-1} \delta_N)\right| \cdots \left|\varphi_{c_0 c_1}^1 \left(A^{-1} \delta_1\right)\right| \\
&\qquad\qquad \left|\hat{r_c}\left(x_{kl} - \delta_N - \cdots - \delta_1\right) - \tilde{r_c}\left(x_{kl} - \delta_N - \cdots - \delta_1\right)\right| \\
&\leq \left(\prod_{k=1}^{N} n_{k-1} p^2 F_k\right) \left\|\tilde{f}_{\theta b}^{-1}(I_j) - I_0\right\|_\infty \\
&\leq \left(\prod_{k=1}^{N} n_{k-1} p^2 F_k\right) \left\|\tilde{f}_{\theta b}^{-1}(I_j) - I_0\right\|_2 .
\end{aligned} \tag{100}$$

Finally, by substituting Eqs. (98) and (100) into Eq. (97), we have

$$\begin{aligned}
&\left\|\tilde{f}_{\theta b}^{-1}(Z_j) - Z_0\right\|_\infty \\
&\leq C_1 h^2 + C_2 p h t^{-1} + \left(\prod_{k=1}^{N} n_{k-1} p^2 F_k\right) \left\|\tilde{f}_{\theta b}^{-1}(I_j) - I_0\right\|_2 .
\end{aligned} \tag{101}$$

If we denote

$$C_3 = \prod_{k=1}^{N} n_{k-1} p^2 F_k, \tag{102}$$

then we can obtain Eq. (95), the proof is then completed. $\square$

B Supplementary Results

In this section, we first provide full-size visualized results of comparison experiments and ablation study in the main text. Fig. 8-11 are the full-size version of comparison results on x4 SyntheticBurst [3] dataset. Fig. 12-15 are the full-size version of comparison results on x4 BurstSR [23] dataset. Fig. 16-18 are the full-size visualized results of ablation study on x4 SyntheticBurst dataset.

In addition, we provide comprehensive multi-scale super-resolution (SR) comparisons on the SyntheticBurst and BurstSR datasets for both ×2 and ×3 scaling factors to further validate the robustness and generalization of our method. Among the compared methods, only BurstM [9] supports multi-scale SR, while other methods exhibit inferior performance compared to both BurstM and our approach. Therefore, we focus our comparison on BurstM as the primary baseline.

The quantitative results are in Table 1 in the main text. The qualitative results on the x2 and x3 SyntheticBurst dataset [3] are presented in Fig. 19 and Fig. 20. The error maps clearly demonstrate that our method achieves superior reconstruction quality, recovering finer details than BurstM. For the x2 and x3 BurstSR dataset [23], as shown in Fig. 21 and Fig. 22, we provide enlarged patches for visual comparison due to the absence of ground truth images. The results highlight that our method preserves more structural information and produces visually sharper results compared to BurstM, further validating its effectiveness in real-world burst SR scenarios. These consistent improvements across datasets and scaling factors underscore the robustness and generalizability of our approach.

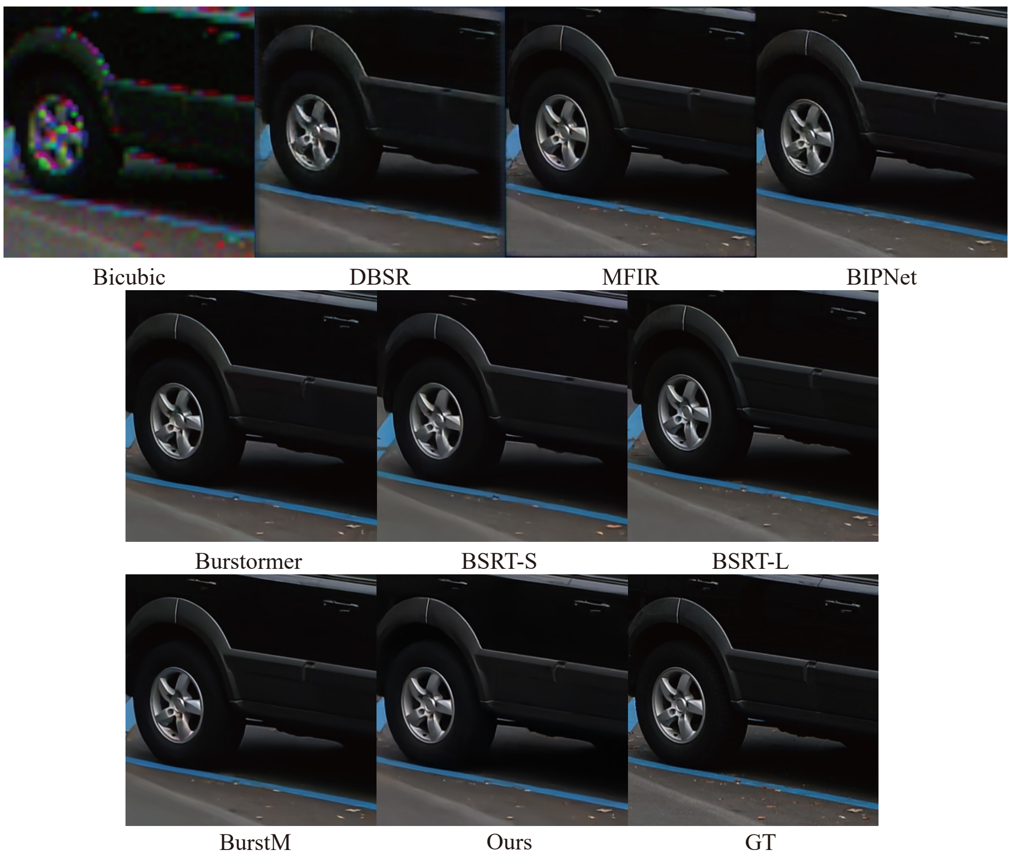

Figure 8: Visual comparison of x4 BISR on the SyntheticBurst dataset.

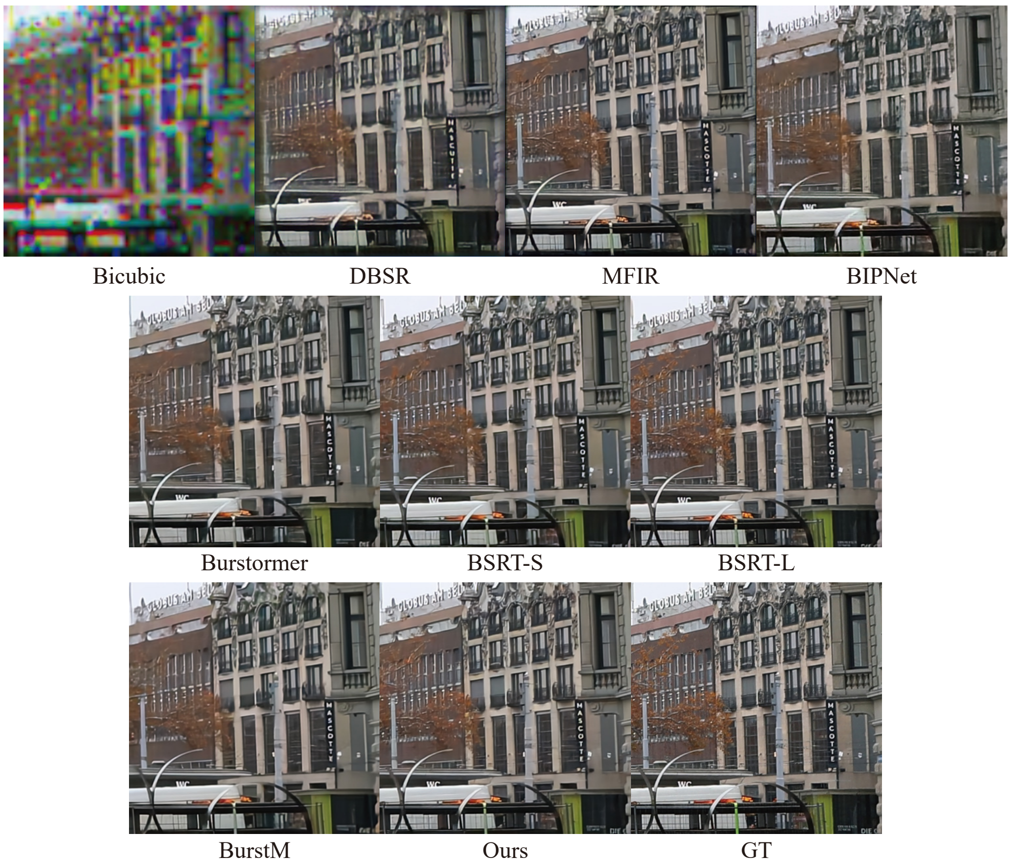

Figure 9: Visual comparison of x4 BISR on the SyntheticBurst dataset.

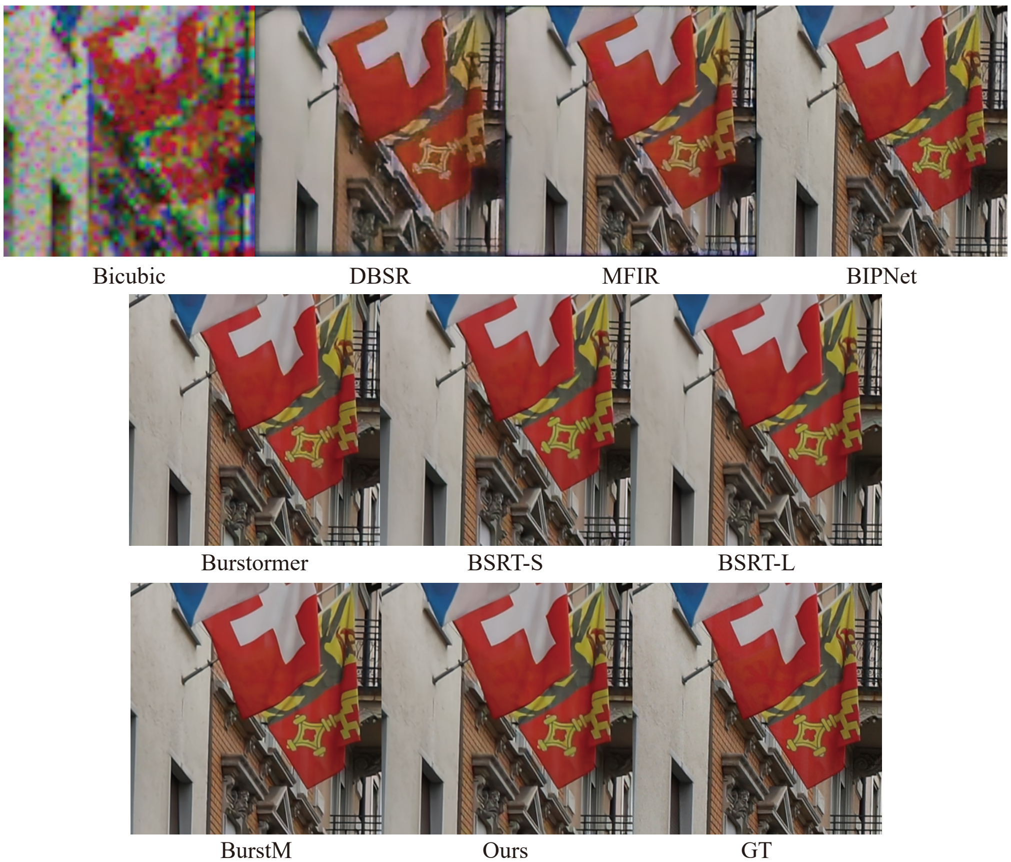

Figure 10: Visual comparison of x4 BISR on the SyntheticBurst dataset.

Figure 11: Visual comparison of x4 BISR on the SyntheticBurst dataset.

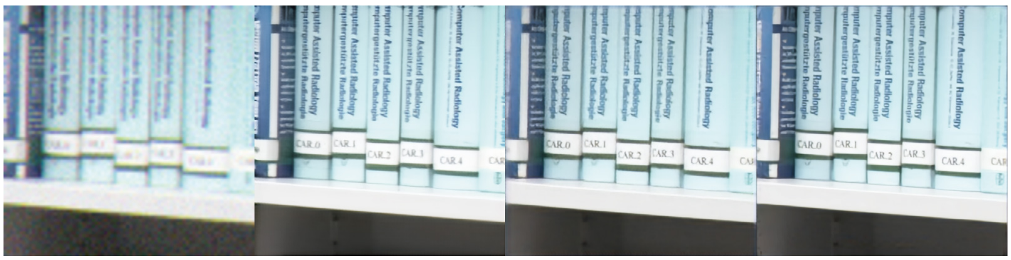

Bicubic DBSR MFIR BIPNet

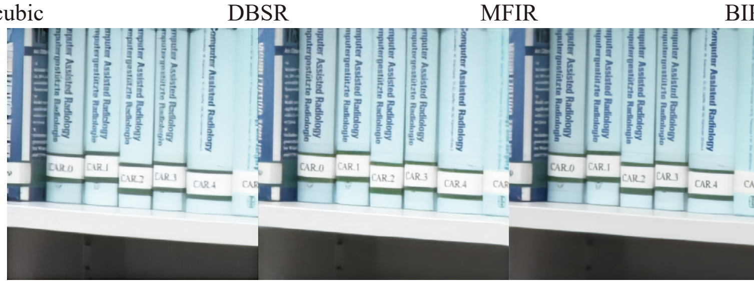

Burstormer BSRT-S BSRT-L

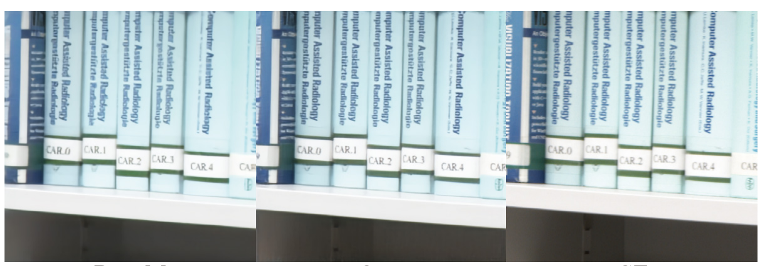

BurstM Ours GT

Figure 12: Visual comparison of x4 BISR on the BurstSR dataset.

Figure 13: Visual comparison of x4 BISR on the BurstSR dataset.

Figure 14: Visual comparison of x4 BISR on the BurstSR dataset.

Bicubic DBSR MFIR BIPNet

Burstormer BSRT-S BSRT-L

Figure 15: Visual comparison of x4 BISR on the BurstSR dataset.

(a) (b) (c)

(d) Ours GT

Figure 16: Visual comparison of ablation study for x4 BISR on the SyntheticBurst dataset.

(a) (b) (c)

(d) Ours GT

Figure 17: Visual comparison of ablation study for x4 BISR on the SyntheticBurst dataset.

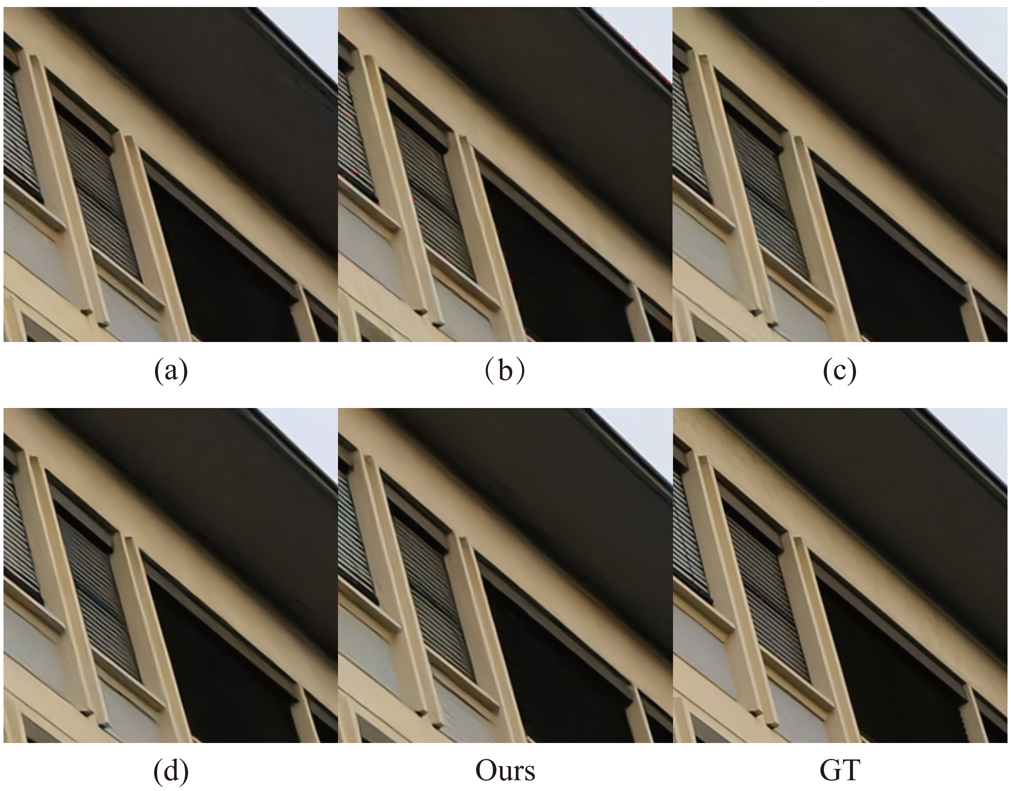

Figure 18: Visual comparison of ablation study for x4 BISR on the SyntheticBurst dataset.

BurstM Ours GT

Figure 19: Visual comparison x2 BISR on the SyntheticBurst dataset.

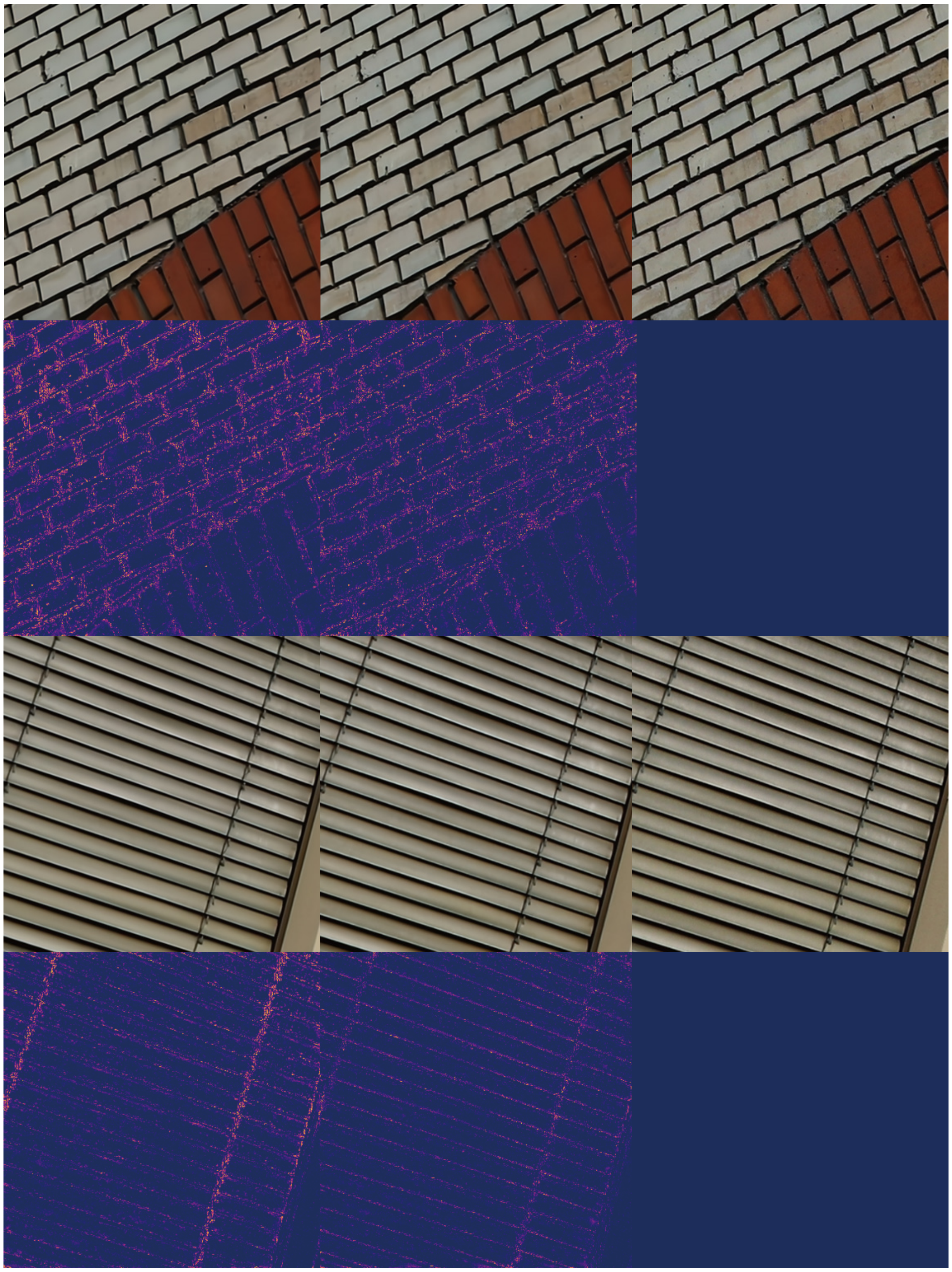

BurstM Ours GT

Figure 20: Visual comparison x3 BISR on the SyntheticBurst dataset.

BurstM Ours GT

Figure 21: Visual comparison x2 BISR on the BurstSR dataset.

Figure 22: Visual comparison x3 BISR on the BurstSR dataset.

NeurIPS Paper Checklist

1. **Claims**

   Question: Do the main claims made in the abstract and introduction accurately reflect the paper's contributions and scope?

   Answer: [Yes]

   Justification:The abstract and introduction clearly state the main contributions of the paper, including both the methodological innovations and the practical improvements.

   Guidelines:

   - The answer NA means that the abstract and introduction do not include the claims made in the paper.
   - The abstract and/or introduction should clearly state the claims made, including the contributions made in the paper and important assumptions and limitations. A No or NA answer to this question will not be perceived well by the reviewers.
   - The claims made should match theoretical and experimental results, and reflect how much the results can be expected to generalize to other settings.
   - It is fine to include aspirational goals as motivation as long as it is clear that these goals are not attained by the paper.

2. **Limitations**

   Question: Does the paper discuss the limitations of the work performed by the authors?

   Answer: [Yes]

   Justification: The limitations are discussed in Section 5 (Conclusion and Limitation), where the authors acknowledge the constraint that the model assumption is limited to the previous development of Eq-CNN.

   Guidelines:

   - The answer NA means that the paper has no limitation while the answer No means that the paper has limitations, but those are not discussed in the paper.
   - The authors are encouraged to create a separate "Limitations" section in their paper.
   - The paper should point out any strong assumptions and how robust the results are to violations of these assumptions (e.g., independence assumptions, noiseless settings, model well-specification, asymptotic approximations only holding locally). The authors should reflect on how these assumptions might be violated in practice and what the implications would be.
   - The authors should reflect on the scope of the claims made, e.g., if the approach was only tested on a few datasets or with a few runs. In general, empirical results often depend on implicit assumptions, which should be articulated.
   - The authors should reflect on the factors that influence the performance of the approach. For example, a facial recognition algorithm may perform poorly when image resolution is low or images are taken in low lighting. Or a speech-to-text system might not be used reliably to provide closed captions for online lectures because it fails to handle technical jargon.
   - The authors should discuss the computational efficiency of the proposed algorithms and how they scale with dataset size.
   - If applicable, the authors should discuss possible limitations of their approach to address problems of privacy and fairness.
   - While the authors might fear that complete honesty about limitations might be used by reviewers as grounds for rejection, a worse outcome might be that reviewers discover limitations that aren't acknowledged in the paper. The authors should use their best judgment and recognize that individual actions in favor of transparency play an important role in developing norms that preserve the integrity of the community. Reviewers will be specifically instructed to not penalize honesty concerning limitations.

3. **Theory assumptions and proofs**

   Question: For each theoretical result, does the paper provide the full set of assumptions and a complete (and correct) proof?

Answer: [Yes]

Justification: All theoretical results in the paper are accompanied by a complete set of clearly stated assumptions and formal proofs. While the full detailed proofs are presented in the Appendix for readability, the main paper includes a simple version to aid understanding.

Guidelines:

- The answer NA means that the paper does not include theoretical results.
- All the theorems, formulas, and proofs in the paper should be numbered and cross-referenced.
- All assumptions should be clearly stated or referenced in the statement of any theorems.
- The proofs can either appear in the main paper or the supplemental material, but if they appear in the supplemental material, the authors are encouraged to provide a short proof sketch to provide intuition.
- Inversely, any informal proof provided in the core of the paper should be complemented by formal proofs provided in appendix or supplemental material.
- Theorems and Lemmas that the proof relies upon should be properly referenced.

4. **Experimental result reproducibility**

Question: Does the paper fully disclose all the information needed to reproduce the main experimental results of the paper to the extent that it affects the main claims and/or conclusions of the paper (regardless of whether the code and data are provided or not)?

Answer: [Yes]

Justification: Yes. The paper provides sufficient details to ensure the reproducibility of its main experimental results. The overall architecture and each individual module are clearly described in Figure 3 and Section 3, offering a comprehensive overview of the proposed method. Furthermore, Section 4.1.1 outlines the experimental settings in detail. These descriptions are sufficient for the reproduction to verify the main claims of the paper.

Guidelines:

- The answer NA means that the paper does not include experiments.
- If the paper includes experiments, a No answer to this question will not be perceived well by the reviewers: Making the paper reproducible is important, regardless of whether the code and data are provided or not.
- If the contribution is a dataset and/or model, the authors should describe the steps taken to make their results reproducible or verifiable.
- Depending on the contribution, reproducibility can be accomplished in various ways. For example, if the contribution is a novel architecture, describing the architecture fully might suffice, or if the contribution is a specific model and empirical evaluation, it may be necessary to either make it possible for others to replicate the model with the same dataset, or provide access to the model. In general. releasing code and data is often one good way to accomplish this, but reproducibility can also be provided via detailed instructions for how to replicate the results, access to a hosted model (e.g., in the case of a large language model), releasing of a model checkpoint, or other means that are appropriate to the research performed.
- While NeurIPS does not require releasing code, the conference does require all submissions to provide some reasonable avenue for reproducibility, which may depend on the nature of the contribution. For example
    (a) If the contribution is primarily a new algorithm, the paper should make it clear how to reproduce that algorithm.
    (b) If the contribution is primarily a new model architecture, the paper should describe the architecture clearly and fully.
    (c) If the contribution is a new model (e.g., a large language model), then there should either be a way to access this model for reproducing the results or a way to reproduce the model (e.g., with an open-source dataset or instructions for how to construct the dataset).
    (d) We recognize that reproducibility may be tricky in some cases, in which case authors are welcome to describe the particular way they provide for reproducibility.

In the case of closed-source models, it may be that access to the model is limited in some way (e.g., to registered users), but it should be possible for other researchers to have some path to reproducing or verifying the results.

5. **Open access to data and code**

   Question: Does the paper provide open access to the data and code, with sufficient instructions to faithfully reproduce the main experimental results, as described in supplemental material?

   Answer: [Yes]

   Justification: We will provide a GitHub repository in the introduction in the de-anonymised version.

   Guidelines:

   - The answer NA means that paper does not include experiments requiring code.
   - Please see the NeurIPS code and data submission guidelines (`https://nips.cc/public/guides/CodeSubmissionPolicy`) for more details.
   - While we encourage the release of code and data, we understand that this might not be possible, so "No" is an acceptable answer. Papers cannot be rejected simply for not including code, unless this is central to the contribution (e.g., for a new open-source benchmark).
   - The instructions should contain the exact command and environment needed to run to reproduce the results. See the NeurIPS code and data submission guidelines (`https://nips.cc/public/guides/CodeSubmissionPolicy`) for more details.
   - The authors should provide instructions on data access and preparation, including how to access the raw data, preprocessed data, intermediate data, and generated data, etc.
   - The authors should provide scripts to reproduce all experimental results for the new proposed method and baselines. If only a subset of experiments are reproducible, they should state which ones are omitted from the script and why.
   - At submission time, to preserve anonymity, the authors should release anonymized versions (if applicable).
   - Providing as much information as possible in supplemental material (appended to the paper) is recommended, but including URLs to data and code is permitted.

6. **Experimental setting/details**

   Question: Does the paper specify all the training and test details (e.g., data splits, hyperparameters, how they were chosen, type of optimizer, etc.) necessary to understand the results?

   Answer: [Yes]

   Justification: All the training and test details are presented in Section 4.1.1 and 4.1.2.

   Guidelines:

   - The answer NA means that the paper does not include experiments.
   - The experimental setting should be presented in the core of the paper to a level of detail that is necessary to appreciate the results and make sense of them.
   - The full details can be provided either with the code, in appendix, or as supplemental material.

7. **Experiment statistical significance**

   Question: Does the paper report error bars suitably and correctly defined or other appropriate information about the statistical significance of the experiments?

   Answer: [No]

   Justification: The experiment for this task is time-consuming. Referring to previous work, there is no need for such experimental data.

   Guidelines:

   - The answer NA means that the paper does not include experiments.

- The authors should answer "Yes" if the results are accompanied by error bars, confidence intervals, or statistical significance tests, at least for the experiments that support the main claims of the paper.
- The factors of variability that the error bars are capturing should be clearly stated (for example, train/test split, initialization, random drawing of some parameter, or overall run with given experimental conditions).
- The method for calculating the error bars should be explained (closed form formula, call to a library function, bootstrap, etc.)
- The assumptions made should be given (e.g., Normally distributed errors).
- It should be clear whether the error bar is the standard deviation or the standard error of the mean.
- It is OK to report 1-sigma error bars, but one should state it. The authors should preferably report a 2-sigma error bar than state that they have a 96% CI, if the hypothesis of Normality of errors is not verified.
- For asymmetric distributions, the authors should be careful not to show in tables or figures symmetric error bars that would yield results that are out of range (e.g. negative error rates).
- If error bars are reported in tables or plots, The authors should explain in the text how they were calculated and reference the corresponding figures or tables in the text.

8. **Experiments compute resources**

   Question: For each experiment, does the paper provide sufficient information on the computer resources (type of compute workers, memory, time of execution) needed to reproduce the experiments?

   Answer: [Yes]

   Justification: The computational cost have been listed in the main text with the used computer workers.

   Guidelines:

   - The answer NA means that the paper does not include experiments.
   - The paper should indicate the type of compute workers CPU or GPU, internal cluster, or cloud provider, including relevant memory and storage.
   - The paper should provide the amount of compute required for each of the individual experimental runs as well as estimate the total compute.
   - The paper should disclose whether the full research project required more compute than the experiments reported in the paper (e.g., preliminary or failed experiments that didn't make it into the paper).

9. **Code of ethics**

   Question: Does the research conducted in the paper conform, in every respect, with the NeurIPS Code of Ethics `https://neurips.cc/public/EthicsGuidelines`?

   Answer: [Yes]

   Justification: We have carefully reviewed the NeurIPS Code of Ethics and confirm that our research fully adheres to its principles.

   Guidelines:

   - The answer NA means that the authors have not reviewed the NeurIPS Code of Ethics.
   - If the authors answer No, they should explain the special circumstances that require a deviation from the Code of Ethics.
   - The authors should make sure to preserve anonymity (e.g., if there is a special consideration due to laws or regulations in their jurisdiction).

10. **Broader impacts**

    Question: Does the paper discuss both potential positive societal impacts and negative societal impacts of the work performed?

    Answer: [No]

Justification: This paper presents work whose goal is to advance the field of Deep Learning and Computer Vision. None of the potential societal consequences we feel must be specifically highlighted here.

Guidelines:

- The answer NA means that there is no societal impact of the work performed.
- If the authors answer NA or No, they should explain why their work has no societal impact or why the paper does not address societal impact.
- Examples of negative societal impacts include potential malicious or unintended uses (e.g., disinformation, generating fake profiles, surveillance), fairness considerations (e.g., deployment of technologies that could make decisions that unfairly impact specific groups), privacy considerations, and security considerations.
- The conference expects that many papers will be foundational research and not tied to particular applications, let alone deployments. However, if there is a direct path to any negative applications, the authors should point it out. For example, it is legitimate to point out that an improvement in the quality of generative models could be used to generate deepfakes for disinformation. On the other hand, it is not needed to point out that a generic algorithm for optimizing neural networks could enable people to train models that generate Deepfakes faster.
- The authors should consider possible harms that could arise when the technology is being used as intended and functioning correctly, harms that could arise when the technology is being used as intended but gives incorrect results, and harms following from (intentional or unintentional) misuse of the technology.
- If there are negative societal impacts, the authors could also discuss possible mitigation strategies (e.g., gated release of models, providing defenses in addition to attacks, mechanisms for monitoring misuse, mechanisms to monitor how a system learns from feedback over time, improving the efficiency and accessibility of ML).

11. **Safeguards**

    Question: Does the paper describe safeguards that have been put in place for responsible release of data or models that have a high risk for misuse (e.g., pretrained language models, image generators, or scraped datasets)?

    Answer: [NA]

    Justification: Our work does not involve pretrained models, generative tools, or scraped datasets that carry a high risk of misuse.

    Guidelines:

    - The answer NA means that the paper poses no such risks.
    - Released models that have a high risk for misuse or dual-use should be released with necessary safeguards to allow for controlled use of the model, for example by requiring that users adhere to usage guidelines or restrictions to access the model or implementing safety filters.
    - Datasets that have been scraped from the Internet could pose safety risks. The authors should describe how they avoided releasing unsafe images.
    - We recognize that providing effective safeguards is challenging, and many papers do not require this, but we encourage authors to take this into account and make a best faith effort.

12. **Licenses for existing assets**

    Question: Are the creators or original owners of assets (e.g., code, data, models), used in the paper, properly credited and are the license and terms of use explicitly mentioned and properly respected?

    Answer: [Yes]

    Justification: We have properly credited all existing assets used in our work, including publicly available datasets and code repositories.

    Guidelines:

    - The answer NA means that the paper does not use existing assets.

- The authors should cite the original paper that produced the code package or dataset.
- The authors should state which version of the asset is used and, if possible, include a URL.
- The name of the license (e.g., CC-BY 4.0) should be included for each asset.
- For scraped data from a particular source (e.g., website), the copyright and terms of service of that source should be provided.
- If assets are released, the license, copyright information, and terms of use in the package should be provided. For popular datasets, `paperswithcode.com/datasets` has curated licenses for some datasets. Their licensing guide can help determine the license of a dataset.
- For existing datasets that are re-packaged, both the original license and the license of the derived asset (if it has changed) should be provided.
- If this information is not available online, the authors are encouraged to reach out to the asset's creators.

13. **New assets**

    Question: Are new assets introduced in the paper well documented and is the documentation provided alongside the assets?

    Answer: [NA]

    Justification: Our paper does not release new assets.

    Guidelines:

    - The answer NA means that the paper does not release new assets.
    - Researchers should communicate the details of the dataset/code/model as part of their submissions via structured templates. This includes details about training, license, limitations, etc.
    - The paper should discuss whether and how consent was obtained from people whose asset is used.
    - At submission time, remember to anonymize your assets (if applicable). You can either create an anonymized URL or include an anonymized zip file.

14. **Crowdsourcing and research with human subjects**

    Question: For crowdsourcing experiments and research with human subjects, does the paper include the full text of instructions given to participants and screenshots, if applicable, as well as details about compensation (if any)?

    Answer: [NA]

    Justification: Our paper does not involve crowdsourcing nor research with human subjects.

    Guidelines:

    - The answer NA means that the paper does not involve crowdsourcing nor research with human subjects.
    - Including this information in the supplemental material is fine, but if the main contribution of the paper involves human subjects, then as much detail as possible should be included in the main paper.
    - According to the NeurIPS Code of Ethics, workers involved in data collection, curation, or other labor should be paid at least the minimum wage in the country of the data collector.

15. **Institutional review board (IRB) approvals or equivalent for research with human subjects**

    Question: Does the paper describe potential risks incurred by study participants, whether such risks were disclosed to the subjects, and whether Institutional Review Board (IRB) approvals (or an equivalent approval/review based on the requirements of your country or institution) were obtained?

    Answer: [NA]

    Justification: Our paper does not involve crowdsourcing nor research with human subjects.

Guidelines:

- The answer NA means that the paper does not involve crowdsourcing nor research with human subjects.
- Depending on the country in which research is conducted, IRB approval (or equivalent) may be required for any human subjects research. If you obtained IRB approval, you should clearly state this in the paper.
- We recognize that the procedures for this may vary significantly between institutions and locations, and we expect authors to adhere to the NeurIPS Code of Ethics and the guidelines for their institution.
- For initial submissions, do not include any information that would break anonymity (if applicable), such as the institution conducting the review.

16. **Declaration of LLM usage**

Question: Does the paper describe the usage of LLMs if it is an important, original, or non-standard component of the core methods in this research? Note that if the LLM is used only for writing, editing, or formatting purposes and does not impact the core methodology, scientific rigorousness, or originality of the research, declaration is not required.

Answer: [NA]

Justification: The core method development in this research does not involve LLMs as any important, original, or non-standard components.

Guidelines:

- The answer NA means that the core method development in this research does not involve LLMs as any important, original, or non-standard components.
- Please refer to our LLM policy (`https://neurips.cc/Conferences/2025/LLM`) for what should or should not be described.